



## Modeling and assessing the impact of tunnel drainage on terrestrial vegetation

Hao Xu, Xiaojun Li\*, Cagri Gokdemir

*Department of Geotechnical Engineering, College of Civil Engineering, Tongji University, 1239 Siping Road, Shanghai 200092, China*



### ARTICLE INFO

**Keywords:**

Tunnel drainage  
Eco-environmental impacts  
Saturated-unsaturated flow  
Quasi-three-dimensional coupling  
Soil–plant–atmosphere continuum

### ABSTRACT

The drainage of mountain tunnels can cause groundwater loss and result in shallow groundwater depletion, which jeopardizes terrestrial vegetation. The impact of tunnel drainage on vegetation can be examined from a physiological perspective using monitoring techniques or evaluated as one item in an environmental assessment of the entire tunnel project. Nevertheless, few previous studies have quantitatively assessed the regional impact of tunnel drainage on plants. We established an assessment framework based on a regionally coupled hydrological model that integrated the tunnel factor into the soil–plant–atmosphere continuum (SPAC) to evaluate the vulnerability status of vegetation threatened by tunnel drainage on a regional scale. The framework comprises five components: (1) a one-dimensional (1D) topsoil model for the vertical unsaturated flow through soil and plants; (2) a three-dimensional (3D) groundwater seepage model delineating water movement between the tunnel and groundwater; (3) a one-way coupling scheme for saturated–unsaturated flow; (4) vegetation-dependent atmospheric boundary conditions representing moisture exchanges between the topsoil and atmosphere; and (5) blockwise vulnerability assessments based on the soil matric potential and vegetation wilting point. The proposed framework was applied to an actual mountain tunnel project. The results showed that the framework can help (i) compare and optimize tunnel design/construction parameters to minimize the impact of tunnel drainage on vegetation, (ii) evaluate the regional impact of long-term/transient drainage of a specific tunnel on plants, and (iii) determine the dominant factor controlling vegetation survival in a given region. Furthermore, the regional impacts of groundwater discharge from the Mingtang Tunnel on vegetation were quantitatively investigated using the assessment framework. It was found that the limited drainage solution of the three typical drainage designs could significantly reduce the area of vulnerable vegetation affected by this tunnel. Groundwater discharge from the Mingtang Tunnel that adopted the limited drainage scheme could harm the growth and yield of vegetation in certain areas, but was unlikely to wither plants, even during drought disasters. In addition, vegetation in this region was more influenced by atmospheric conditions than tunnel drainage. The proposed method can provide a novel perspective and practical assessment tool for promoting environmentally friendly tunnel engineering.

### 1. Introduction

Tunnels have been extensively used for the development of transportation infrastructure such as highway and railway projects, especially in mountainous areas. Concerns about the negative environmental impacts of tunnels have grown as environmental protection concepts have become increasingly prevalent (van Geldermalsen, 2004; Sweetnam et al., 2017). Because tunnels are often surrounded by groundwater, their drainage may change groundwater flow patterns (Zaide et al., 2010) and cause groundwater decline (Yoo, 2005; Moon &

Fernandez, 2010), further affecting surface hydrological processes (Gargini et al., 2008; Vincenzi et al., 2009; Raposo et al., 2010) and threatening the surrounding eco-environment (Kværner & Snilsberg, 2011; Li et al., 2016). For example, the maximum groundwater inflow into the Zhongliangshan Tunnel of the Xiang-Yu Railway reached 54,100 m<sup>3</sup>/d, which resulted in the drying up of 48 wells and declines in the water levels of over 100 wells and springs (Zheng et al., 2017). Moreover, the Huayingshan Tunnel of the Guang-Yu Highway discharged approximately  $730 \times 10^4$  m<sup>3</sup> of groundwater annually, accounting for 44% of the annual groundwater recharge in this region,

\* Corresponding author.

E-mail address: [lixiaojun@tongji.edu.cn](mailto:lixiaojun@tongji.edu.cn) (X. Li).

which dried up springs, unbalanced the water circulation, and caused severe soil erosion (Liu et al., 2001).

In projects similar to those described above, vegetation, which is a vital component of the eco-environment, can also be imperiled by tunnel-induced groundwater decline (Lv et al., 2020). Consequently, the ecosystem services (Daily, 1997; Millennium Ecosystem Assessment, 2005) provided by plants, including climate regulation, soil erosion control, habitat provision, and food/material production (Krieger, 2001; García-Nieto et al., 2013), can also be adversely affected by groundwater discharge, which may become a concern for underground space planning (Bobylev, 2018). In more severe cases, the detrimental effects of tunnel drainage on plants can escalate to damage to the surrounding ecosystem (Kværner & Snilsberg, 2008) and local agriculture (Fais & Nino, 2004; Wei & Pan, 2011). Accordingly, modeling and assessing tunnel drainage impacts on vegetation will facilitate the inclusion of ecosystem service considerations in underground space planning and promote more environmentally friendly tunnel engineering.

Previous studies have primarily examined the impact of tunnel drainage on vegetation based on long-term monitoring and on-site tests. By monitoring variations in tree ring width, it was found that tunnel excavation reduced vegetation growth rates for 15 y after construction (Zheng et al., 2017). The isotopic analysis ( $\delta^{2}\text{H}$  and  $\delta^{18}\text{O}$ ) conducted by Liu et al. (2019) indicated that groundwater decline caused by tunnel drainage led to a transformation in plant water absorption patterns. Remote sensing techniques have also been utilized to analyze changes in vegetation coverage before and after tunnel construction (Fais & Nino, 2004; Wei & Pan, 2011). However, the heavy dependence on monitoring or field tests makes these approaches less applicable during the planning and design stages of tunnel projects.

Before excavation, the eco-environmental influences of tunnel projects are often evaluated through environmental impact assessments (EIA), strategic environmental assessments (SEA), life cycle assessments (LCA), and sustainability assessments (SA). For example, Namin et al. (2014) and Phillips (2016) considered tunnel-caused interference with surface/underground water in an EIA. Zhang et al. (2012) adopted the dewatering funnel area and surface runoff as indexes to evaluate the water ecological effect of tunnel engineering. Liu et al. (2015) combined geological, hydrological, and tunnel indicators to assess the negative effects of tunneling on the groundwater environment. Xu et al. (2016) analyzed the impact of groundwater level drawdown caused by underground works on the geological environment based on the view of SEA, which can evaluate the environmental impacts of policies, plans, and programs for underground infrastructure at a strategic level (Bobylev, 2006). Moreover, Huang et al. (2015) and Audi et al. (2020) evaluated the environmental impacts (e.g., global climate and human toxicity) of each phase in the whole-life cycle of a tunnel following the principles of LCA. Some SA cases for tunneling or underground space development have also included environmental factors such as greening, vegetation community restoration, biodiversity, and water resources/supply (Qiu et al., 2020; Zargarian et al., 2016).

Although many assessments have considered the eco-environmental influences of tunnel projects, to the best of our knowledge, few have focused on the tunnel-induced impacts on vegetation. Moreover, most previous assessments have understated the hydraulic connections and ecological feedback between underground structures, groundwater, soil, plants, and the atmosphere. Hence, the integrated tunnel-vegetation assessment framework in this study may expand the application scope of environmental assessments (EA) in tunnel engineering and improve the theoretical system of existing EA methods.

To quantify the impact of tunnel drainage on vegetation, Gokdemir et al. (2019) proposed an assessment method that integrated the tunnel factor into the soil-plant-atmosphere continuum (SPAC). SPAC regards the soil, plants, and atmosphere as a dynamic physical system in which water transfers freely between components until a balance is reached (Philip, 1966). However, classical SPAC models have paid little attention to the hydraulic influences of subsurface structures on the

environment, making it difficult for them to evaluate the impact of tunnel drainage on vegetation (Gokdemir et al., 2019; Li et al., 2020). To introduce the tunnel factor into the SPAC, Gokdemir et al. (2019) input the maximum stable groundwater level after tunnel construction into a one-dimensional (1D) hydrological model as the bottom boundary condition. By failing to account for the regional groundwater environment, the method only evaluated ecological influences at specific sites where the maximum groundwater drawdown occurred instead of over the entire research region. In addition, the method did not consider groundwater fluctuations during tunneling.

This study followed the tunnel-SPAC integration scheme and extended the original assessment method to a regional framework using a quasi-3D hydrological numerical model. The quasi-3D model coupled the 1D unsaturated flow and 3D groundwater seepage (Abbott et al., 1986; Seo et al., 2007; Mao et al., 2019) based on two developed hydrological models: Hydrus-1D (Šimunek et al., 2009) and Modflow-NWT (Niswonger et al., 2011). The topsoil model (Hydrus-1D) simulated the vertical unsaturated flow and dynamic root wilting within the vadose zone. The groundwater model (Modflow-NWT) simulated the 3D groundwater seepage affected by tunnel drainage. The coupling between the topsoil and groundwater models was conducted using a one-way method (Zeng et al., 2019), which delivered the groundwater levels to the topsoil model as bottom boundary conditions (BCs) (Hanson et al., 2014; Markstrom et al., 2008; Xu et al., 2012). In addition, we used atmospheric BCs at the top of the quasi-3D model to represent the moisture exchange between the atmosphere and land. The atmospheric BCs were calculated based on the Penman-Monteith equation and varied with the vegetation growth stages. The entire research area was divided into multiple blocks, and in each block, the vertical distribution of the soil matric potential ( $h$ ) was computed using the 1D topsoil model. The framework evaluated the regional vegetation vulnerability status through a blockwise comparison between  $h$  and the wilting point.

The assessment framework was applied to an actual highway tunnel to validate its applicability. The results indicated that this framework had several contributions:

- (1) The framework can help compare and optimize tunnel design/construction parameters (such as drainage design criteria and excavation speeds) to reduce the influence of tunnel drainage on vegetation.
- (2) The framework can evaluate the regional impact of tunnel drainage on vegetation during or after construction. Both normal and extreme atmospheric conditions are included in the assessments.
- (3) The framework can elucidate the interaction between environmental factors and determine which factors control vegetation survival.

The remainder of this paper is organized as follows: Section 2 introduces the tunnel-SPAC integration and the criteria used to evaluate the vulnerability status of vegetation. Section 3 presents the regional assessment framework and focuses on the quasi-3D numerical model. The case study of the assessment framework is presented in Section 4, followed by a summary and conclusions in Section 5.

## 2. Vulnerability of vegetation against tunnel drainage

This section summarizes our recent studies (Gokdemir et al., 2019; Li et al., 2020), which comprise two parts: (1) the integration of the tunnel and SPAC and (2) the criteria used to evaluate when plants affected by tunnel drainage become vulnerable.

### 2.1. Integration of the tunnel and SPAC

The SPAC is a dynamic physical system in which water transfers freely between components until a balance is reached (Philip, 1966). As

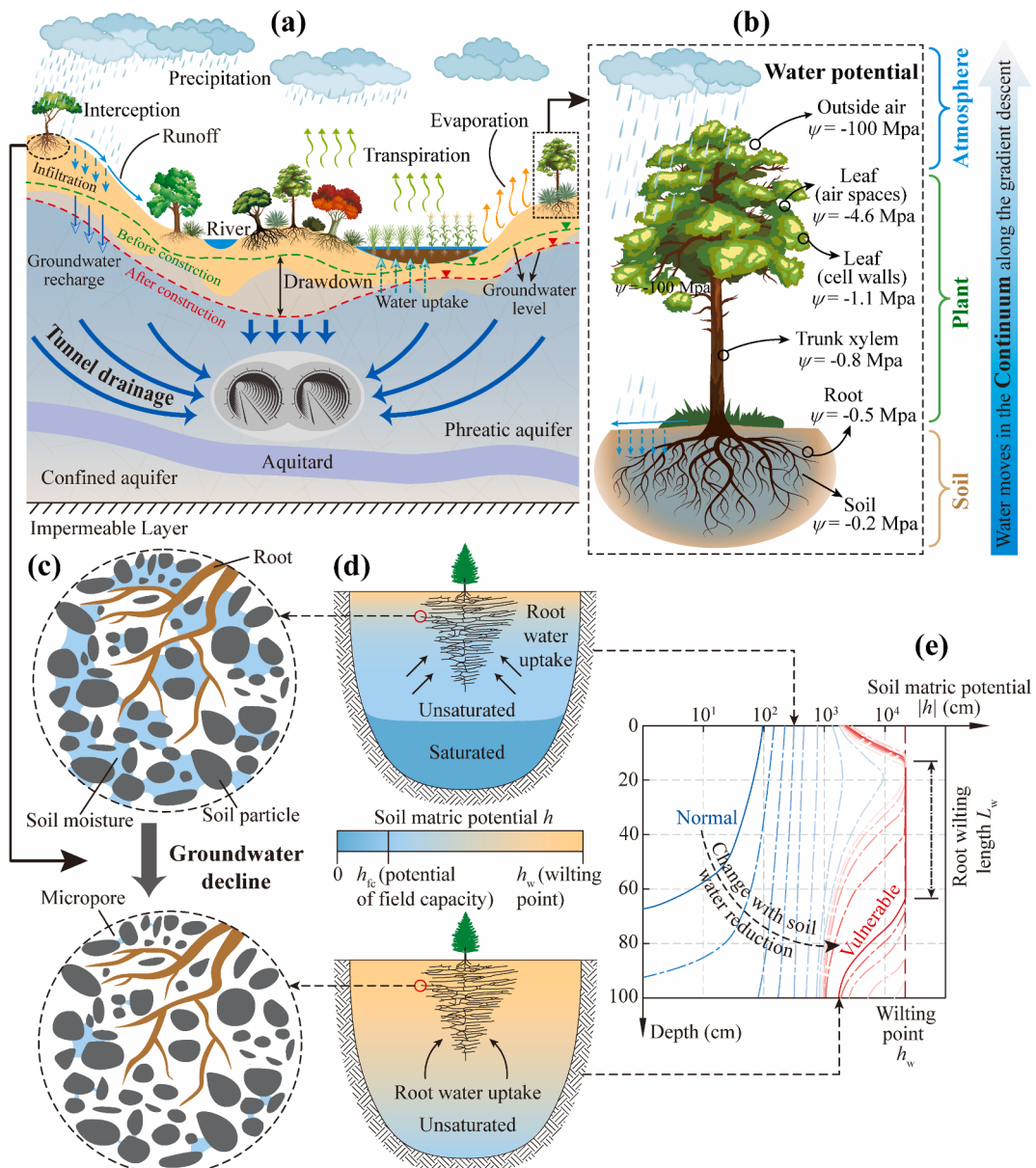


**Fig. 1.** (a) Water transfer among components of the tunnel-SPAC integration (Ward & Trimble, 2003); (b) typical water potential values of SPAC components and water movement direction in SPAC (McElrone et al., 2013); (c) capillary break within the micro-porosity of the rhizosphere; (d) changes in the soil matric potential after groundwater decline; (e) with the gradual consumption of soil water,  $h$  along the soil profile ( $D_r$  is assumed to be 1 m) approaches  $h_w$ , and the length of roots that wilt ( $L_w$ ) increases accordingly.

shown in the upper part (above groundwater) of Fig. 1(a), a typical SPAC system delineates water movements among soil, plants, and the atmosphere, which constitute various surface hydrological processes and play important roles in the surface water cycle. Through the word continuum, SPAC highlights the continuity and integrity of water transfer across the soil–plant, soil–atmosphere, and plant–atmosphere interfaces.

The water movement is driven by the gradient in the water potential, i.e., water always moves from higher to lower water potentials (Robinson & Ward, 2017). As shown in Fig. 1(b), in a SPAC system, the water potential difference between air and leaves pushes moisture in the leaves to vaporize through the stomata; then, moisture in the branch and trunk parts of plants will be extracted to the canopy to supplement the leaf water loss. This force, called transpiration pull, will then be transmitted down through the plant, finally extracting water from the soil through the roots (Nemali & Stephens, 2014; McElrone et al., 2013).

However, classical SPAC models, such as CoupModel (Jansson, 2012), SWAP (Kroes et al., 2017), and SWAT (Arnold et al., 1998),

which focus on simulating surface hydrological processes, have generally treated the groundwater seepage field as the bottom BC of the surface water circulation and have paid little attention to the perturbation of the groundwater environment caused by underground structures. To integrate the tunnel factor into the SPAC, we introduced tunnel–groundwater and groundwater–soil connections into the system, as shown in the lower part of Fig. 1(a) (below the water level). These improvements enable the SPAC system to consider the hydraulic and ecological influences exerted by substructures on terrestrial vegetation through groundwater.

## 2.2. Indicator to represent the water deficit of vegetation

We introduced the soil matric potential as an indicator to measure the availability of soil water to plants. The soil matric potential (also known as soil water pressure head),  $h$ , an essential component of the soil water potential, constitutes the suction force with which water is held by

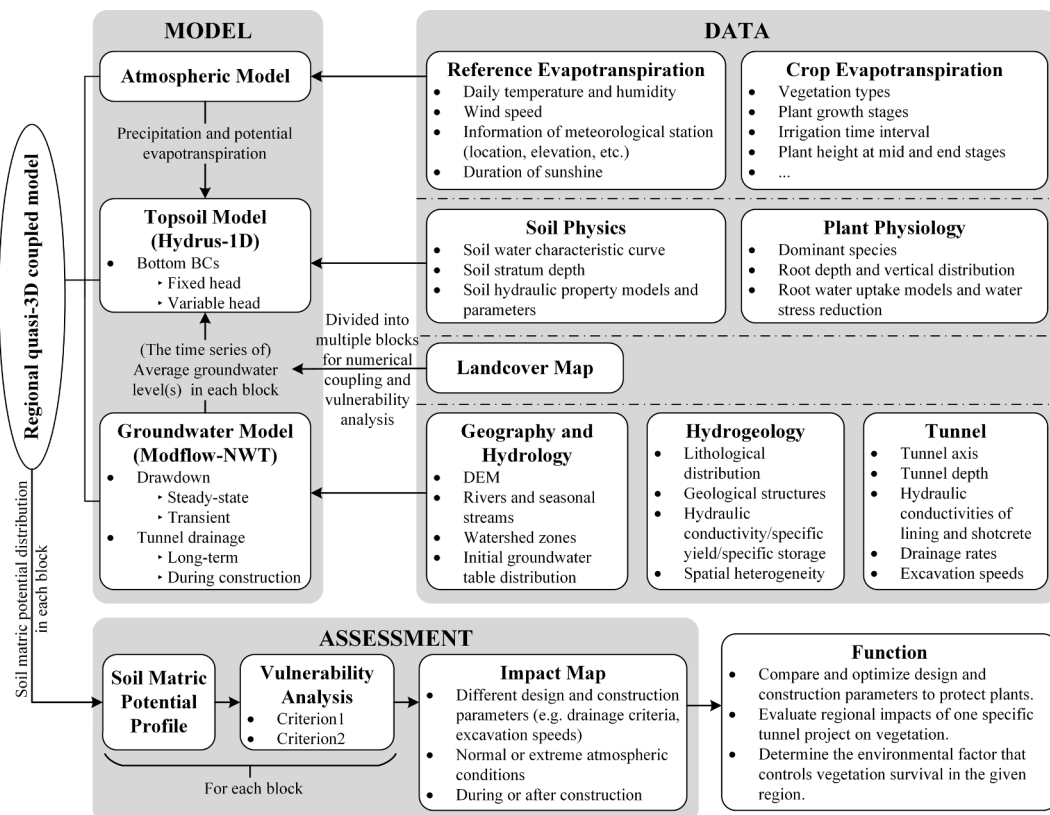


**Fig. 2.** Schematic diagram of the regional assessment framework.

the soil matrix (soil particles and pore spaces); the soil matric potential is negative within the unsaturated zone and zero under the groundwater level (Hanks, 1992; Yadavinder-Singh et al., 2014).

When tunnel drainage leads to groundwater decline, soil water within the root zone can gradually be consumed by plant transpiration and soil evaporation because its hydraulic connection with the groundwater has been broken. As soil dry-down progresses, it becomes increasingly difficult for plant roots to extract water from the soil. Plants experience water stress when water extraction from the roots is less than the water loss from plants determined by the evaporative demand of the atmosphere (Nemali & Stephens, 2014). Under water stress, plants suffer from many detrimental effects at the molecular, metabolic, and physiological levels, such as gene expression changes, cell growth reduction, abnormal metabolite accumulation, stomatal closure, lower carbon metabolism, and crop yield decreases (Nemali & Stephens, 2014; Porporato et al., 2001; Hsiao, 1973). When soil water is almost depleted, as shown in Fig. 1(c), a capillary break occurs within the micropores of the root zone. As a result, the roots are unable to extract moisture from the soil, thus driving plants into a wilting situation (Assi et al., 2019).

From the perspective of water energy, a decrease in soil water content also reduces the soil matric (water) potential. As shown in Fig. 1(d), with the gradual consumption of soil moisture, the soil matric potential will decrease to the wilting point, i.e., the matric potential during vegetation wilting. At this point, water is held by soil particles at a pressure much greater than the standard atmospheric pressure; therefore, it is unavailable for extraction by roots.

### 2.3. Vulnerability criteria

Two criteria were defined to judge the vulnerability status of vegetation based on the vegetation wilting point. The first criterion defines any condition that drops the soil matric potential to the wilting point as vulnerable. However, minor drying of the roots will not wither the

whole plant (Consoli et al., 2017). After groundwater decline, with the loss of soil water, the vegetation gradually withers, and the length of roots that wilt expands progressively (Fig. 1(e)). Here, we used the percentage ratio of the root wilting length ( $L_w$ ) over the entire rooting depth ( $D_r$ ) to represent the partial drying of vegetation roots.  $L_w$  refers to the vertical length of roots where the adjacent soil has a matric potential reaching the wilting point. The whole vegetation was assumed to wither after  $L_w$  reached more than half of  $D_r$  (Gokdemir et al., 2019). Hence, the second criterion for the vulnerability status of the plants was defined as  $L_w/D_r = 50\%$ .

### 3. Assessment framework

This section introduces a regional assessment framework to evaluate the impact of tunnel drainage on vegetation based on a quasi-3D coupled hydrological numerical model.

#### 3.1. Overview of the framework

Fig. 2 shows a schematic diagram of the regional assessment framework. The workflow of this framework consists of three main steps: preparing data, building numeric models, and assessing impacts. In the data preparation phase, both in-situ and ex-situ information can be used owing to the limitations of field tests. In the modeling phase, a one-way coupled quasi-3D numerical model combines the 3D groundwater model with the 1D topsoil model. During coupling, for each block of the land cover map, groundwater tables of nodes within the block are averaged and delivered to the corresponding topsoil part as bottom BCs. In addition, the atmospheric forcing is related to the plant types and growth stages. After computing the soil matric potential distribution, the regional influence of tunnel drainage on vegetation can be assessed by conducting a vulnerability analysis in each block of the study area.

### 3.2. Quasi-3D coupled numerical model

The quasi-3D model consists of three sub-models: (1) the atmospheric model representing moisture exchange between the topsoil and atmosphere; (2) the 3D groundwater seepage model that delineates water transfer between the tunnel and groundwater; and (3) the 1D topsoil model simulating the vertical unsaturated flow in the vadose zone. The following sections summarize the governing equations for each model.

#### 3.2.1. Atmospheric model

The atmospheric model provides atmospheric forcing (top BCs) for the quasi-3D model. The atmospheric forcing contains three components: potential evaporation,  $E_p$ ; potential transpiration,  $T_p$ ; and precipitation,  $P$ . We used the method suggested by the FAO (Allen et al., 1998) and ASCE (Jensen & Allen, 2016) to calculate the potential evapotranspiration,  $ET_p (=E_p + T_p)$ :

$$ET_p = K_c \times ET_o \quad (1)$$

where  $K_c$  is the crop coefficient, which varies with the crop growth stages (-), and  $ET_o$  is the reference evapotranspiration (L) derived from the Penman–Monteith equation (Zotarelli et al., 2010).

$ET_p$  is divided into  $E_p$  and  $T_p$  based on the Beer–Lambert law, which partitions the solar radiation via interception by the canopy (Ritchie, 1972; Belmans et al., 1983). The partitioning equations are summarized as follows:

$$\left\{ \begin{array}{l} E_p = ET_p \cdot \exp(-k \cdot LAI) T_p = ET_p \cdot (1 - \exp(-k \cdot LAI)) \end{array} \right. \quad (2)$$

where  $k$  is the extinction coefficient (-), and  $LAI$  is the leaf area index (-).

#### 3.2.2. Groundwater seepage model

The groundwater model takes advantage of the Modflow-NWT to simulate the groundwater seepage field affected by tunnel drainage. Modflow is a modular three-dimensional groundwater model that simulates groundwater flow by utilizing the equivalent porous medium assumption and the cell-centered finite-difference approach (Harbaugh, 2005). Modflow-NWT is a variant of Modflow and is specially designed to solve problems involving unconfined aquifers and the interaction between surface water and groundwater (Niswonger et al., 2011).

The governing equations of the groundwater model solved by Modflow-NWT are as follows:

$$\nabla \cdot (K_s \nabla H) + W = \begin{cases} 0, \text{ steady-state} \\ \mu_s \frac{\partial H}{\partial t}, \text{ transient} \end{cases} \text{ s.t. } \begin{cases} H = H_0, t = t_0 \\ (K_s \nabla H)|_{\Gamma_1} = 0, t > t_0 \\ H|_{\Gamma_2} = H_0|_{\Gamma_2}, t > t_0 \\ H|_{\Gamma_3} = Ele|_{\Gamma_3}, t > t_0 \end{cases} \quad (3)$$

where  $\nabla = \frac{\partial}{\partial x} + \frac{\partial}{\partial y} + \frac{\partial}{\partial z}$ ,  $K_s$  is the saturated hydraulic conductivity ( $LT^{-1}$ ),  $W$  is the volumetric flux per unit volume representing sources and/or sinks of water ( $T^{-1}$ ),  $\mu_s$  is the specific storage in a confined layer or the specific yield in an unconfined layer ( $L^{-1}$ ),  $H$  is the hydraulic head (L),  $t$  is time (T),  $H_0$  is the initial hydraulic head (L),  $t_0$  represents the starting time of the simulations (T),  $\Gamma_1$  is the bottom of the model,  $\Gamma_2$  is the periphery of the study site,  $\Gamma_3$  represents rivers or streams, and  $Ele$  is the elevation (L). The influences of various hydrological processes (Fig. 1(a)) on the groundwater system were simplified to the BCs of Eq. (3) or assembled in the term  $W$ .

(I) Groundwater recharge from precipitation is generally less than the total rainfall due to canopy interception, surface runoff, soil storage, etc. (Pan et al., 2017). A reduction coefficient,  $\lambda$ , known as the recharge–precipitation ratio, was used to represent the loss of rainfall, and the rainfall recharge was modeled as follows (Rangarajan & Athavale, 2000; Li et al., 2018):

$$W_{RCH} = \lambda \cdot P \quad (4)$$

(II) According to the assumptions of Harbaugh (2005), evapotranspiration ( $ET$ ) reaches the maximum value when the water table is at or above the ground surface, decreases linearly with the decline in water level, and ceases when the water level drops below a specified depth, termed the extinction depth. The maximum evapotranspiration can be modeled as follows:

$$(W_{EVT})_{\max} = \xi \cdot ET_o \quad (5)$$

where  $\xi$  is an empirical factor that adjusts  $ET_o$  by considering the effects of land cover types and vegetation growth stages.

In Eqs. (4) and (5), water is directly recharged to or removed from the groundwater system, no water movement (e.g., infiltration or percolation) within the unsaturated zone is considered, and the effect of soil moisture changes on  $ET$  is also neglected. These simplifications can be applied to steady-state simulations because the time term is excluded from Eq. (3) in these cases. However, the role of the topsoil becomes non-negligible during transient analyses.

(III) In transient analyses, the unsaturated-zone flow (UZF) package of Modflow was introduced to simulate vertical water flow through the topsoil and calculate the actual rainfall recharge and  $ET$ . The governing equation is given as follows (Niswonger et al., 2006):

$$\frac{\partial \theta}{\partial t} + \frac{\partial K(\theta)}{\partial z} + i = 0, \quad (6)$$

where  $\theta$  is the soil volumetric water content (-);  $K(\theta)$  is the unsaturated hydraulic conductivity ( $LT^{-1}$ ), which is expressed as a function of  $\theta$  and described using the Brooks–Corey model (1964);  $z$  is the vertical coordinate (L); and  $i$  is the evapotranspiration rate per unit depth ( $T^{-1}$ ). Eq. (6) is a simplified 1D Richards equation excluding the diffusive term and sink/source term; it assumes that the vertical flow is driven only by gravitational forces.

(IV) Heavy rainfall may cause surface runoff after depressions on the ground surface are filled or the soil becomes saturated. Surface runoff can move downslope as overland flow or converge in streams as streamflow, eventually routing to rivers and flowing out of the watershed (Ward & Trimble, 2003). The groundwater model does not simulate processes of runoff yield and concentration, but sets drainage BCs at the ground surface to consider the role of runoff in removing ponding. It is assumed that surface ponding is drained instantaneously.

(V) The model also considers the groundwater regulation functions of rivers and streams. If groundwater levels rise above rivers, groundwater will be discharged into the rivers. Conversely, rivers will supply water to the groundwater system.

The groundwater inflow into a tunnel can be expressed as follows (Toran & Bradbury, 1988; Adams & Younger, 2001; Zaidel et al., 2010; Butscher, 2012):

$$q_{in} = \begin{cases} \beta K_{rock} (H|_{\Gamma_4} - Ele|_{\Gamma_4}), & H|_{\Gamma_4} \geq Ele|_{\Gamma_4} \\ 0, & H|_{\Gamma_4} < Ele|_{\Gamma_4} \end{cases} \quad (7)$$

where  $K_{rock}$  is the hydraulic conductivity of the surrounding rock mass contiguous to the tunnel ( $LT^{-1}$ ),  $\beta$  is the drainage coefficient that represents the integral drainage ability of the lining layer and the tunnel drainage system, and  $\Gamma_4$  represents the interface between the tunnel opening and the surrounding rock.

#### 3.2.3. Topsoil model

The topsoil model simulates vertical unsaturated flow and the distribution of the soil matric potential within the vadose zone using Hydrus-1D. Hydrus-1D is a one-dimensional finite element model for analyzing water flow and solute transport in variably saturated porous media (Šimůnek et al., 2009). In Hydrus-1D, the vertical unsaturated flow within the vadose zone is governed by the 1D Richards equation, as follows:

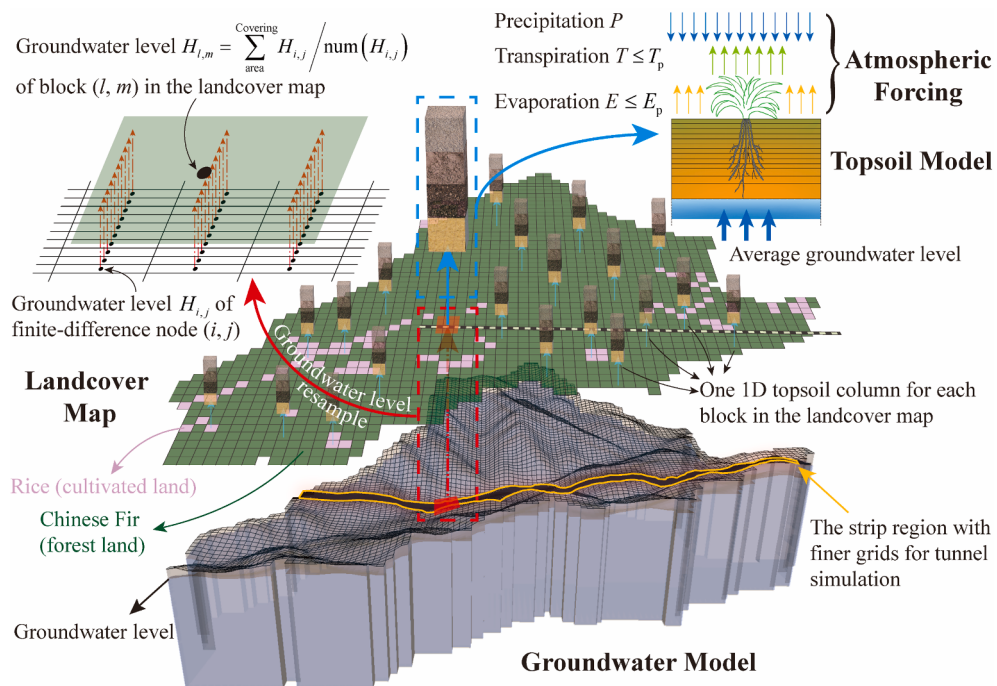


Fig. 3. Schematic diagram of the quasi-3D one-way coupling scheme.

$$\frac{\partial \theta(h)}{\partial t} = \frac{\partial}{\partial z} \left[ K(h) \left( \frac{\partial h}{\partial z} + 1 \right) \right] - S(h, z, T_p) \text{ s.t.,} \quad (8)$$

$$\begin{cases} h = h_0, t = t_0 & (9) \\ \left| \left[ K(h) \left( \frac{\partial h}{\partial z} + 1 \right) - \partial_z S(h, z, T_p) \right] \right|_{z=z_0} \leq |P - E_p|, t > t_0 & (10) \\ h_{\min} \leq h|_{z=z_0} \leq 0, t > t_0 & (11) \\ h|_{z=z_{GWL}} = 0, t > t_0 & (12) \end{cases}$$

where  $h$  is the soil matric potential (L);  $\theta(h)$  is the soil volumetric water content, expressed as a function of  $h$  (-);  $K(h)$  is the unsaturated hydraulic conductivity ( $\text{LT}^{-1}$ );  $S(h, z, T_p)$  is the sink/source term, representing root water uptake herein ( $\text{T}^{-1}$ );  $z_0$  and  $z_{GWL}$  denote the vertical coordinates of the ground surface and groundwater level, respectively (L); and  $h_{\min}$  is the allowable minimum soil matric potential at the soil surface, which is determined from the equilibrium conditions between the soil water and atmospheric water vapor (L). Based on the requirements of Eqs. (10) and (11), the atmospheric BCs are converted between Dirichlet, Neumann, and Robin BCs to maximize the absolute value of the flux through the soil surface (Neuman et al., 1975).

The hydraulic properties of the unsaturated zone are described using the soil water retention equation,  $\theta(h)$ , introduced by van Genuchten (1980) in combination with the pore size distribution model proposed by Mualem (1976) for the unsaturated hydraulic conductivity,  $K(h)$ .  $\theta(h)$  is given by the following:

$$\theta(h) = \begin{cases} \theta_r + \frac{\theta_s - \theta_r}{[1 + |\alpha h|^n]^m}, h < 0 \\ \theta_s, h \geq 0 \end{cases}, \quad (13)$$

where  $\theta_r$  and  $\theta_s$  are the residual and saturated water contents (-), respectively;  $\alpha$  is related to the inverse of the air-entry pressure (-2 cm in this study);  $n$  is a measure of the pore size distribution; and  $m = 1 - 1/n$ .  $K(h)$  can be modeled as follows:

$$K(h) = K_s S_e^l \left[ 1 - \left( 1 - S_e^{1/m} \right)^m \right]^2 \quad (14)$$

where  $l$  is an empirical pore-connectivity parameter, and  $S_e$  is the

effective saturation given by

$$S_e = \frac{\theta(h) - \theta_r}{\theta_s - \theta_r}. \quad (15)$$

The root water-uptake term,  $S(h, z, T_p)$ , was modeled using the method proposed by Feddes et al. (1978), formulated as follows:

$$S(h, z, T_p) = \delta(h) S_p(z) \quad (16)$$

$$\delta(h) = \begin{cases} 0, h \leq h_w \text{ or } h \geq h_1 \\ \frac{h - h_1}{h_2 - h_1}, h_2 < h < h_1 \\ 1, h_3 < h < h_2 \\ \frac{h - h_w}{h_3 - h_w}, h_w < h < h_3 \end{cases}, \quad (17)$$

$$S_p(z) = \frac{R(z_r)}{\int_0^1 R(z_r) dz_r} T_p, \quad (18)$$

where  $\delta(h)$  is the reduction function of root water uptake, also known as the water stress response function;  $h_1$  is the anaerobiosis point (L);  $h_2$  and  $h_3$  are matric potentials between which root water uptake maintains the maximum rate (L);  $S_p(z)$  is the potential root water uptake rate ( $\text{T}^{-1}$ ); and  $R(z_r)$  is the root length density ( $\text{L}^{-2}$ ) as a function of the relative depth,  $z_r (= z/D_r)$ .  $R(z_r)$  can be modeled using the method proposed by Santos et al. (2017):

$$R(z_r) = \frac{b^2 R_{\text{avg}}}{b + e^{-b} - 1} (1 - z_r) e^{-b z_r}, \quad (19)$$

where  $R_{\text{avg}}$  is the average root length density of plants, and  $b$  is a shape-factor parameter. More information about the topsoil model is provided by Gokdemir et al. (2019) and Li et al. (2020).

### 3.2.4. Coupling scheme

Fig. 3 depicts the coupling scheme for combining the three sub-models discussed above. A one-way method was adopted to couple the unsaturated flow (the topsoil model) and the saturated flow (the groundwater model). When combining multiple sub-models, the one-

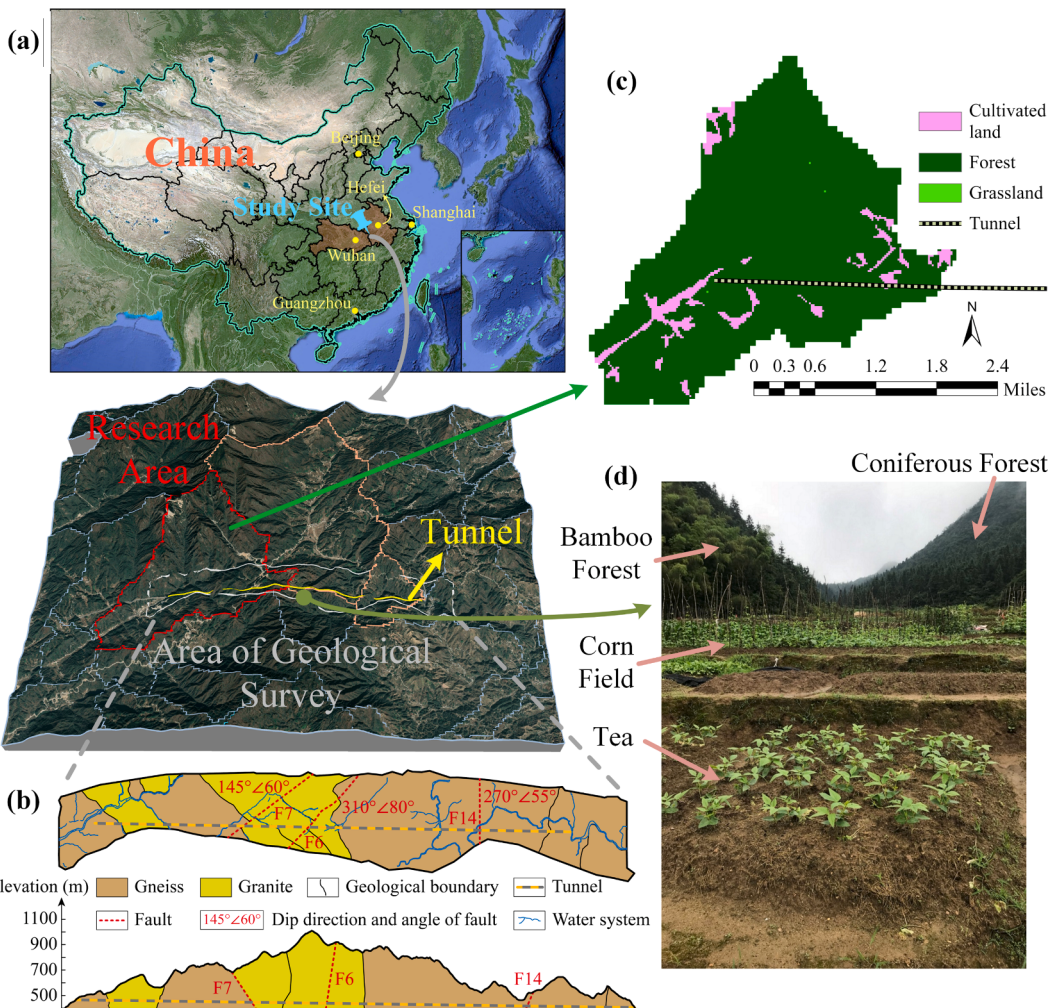


**Fig. 4.** (a) Geographic location of the study site. (b) Geological diagrams of the belt area adjacent to the Mingtang Tunnel (Li et al., 2018). The upper and lower diagrams provide a planar view and longitudinal section along the tunnel axis, respectively. (c) Land cover map of the research area. (d) Representative plants in the study site (Gokdemir et al., 2019).

way coupling scheme unidirectionally delivers the solutions of one sub-model to another sub-model, instead of using the feedback mechanism to exchange messages between the sub-models at the interface nodes (two-way coupling) or solving the assembled matrices of the sub-models (fully coupling) (Zeng et al., 2019). In our case, the one-way coupling scheme delivered groundwater levels from the groundwater model to the topsoil model as bottom BCs, neglecting the feedback from the topsoil (water recharge or consumption) to the groundwater.

Before coupling, the topsoil was conceptualized into multiple parallel soil “columns” having no lateral flow, and each column matched one block in the landcover map. Considering that the size of some grids in the groundwater model might be much smaller than the area represented by a topsoil column, groundwater levels were resampled into the corresponding block, as shown in Fig. 3. During resampling, the groundwater levels of all nodes lying within the coverage of one block were counted and averaged. The average groundwater table after processing was then delivered to the corresponding topsoil column as the bottom BCs.

During the coupling of steady-state cases, only one average groundwater table in each block, representing the long-term stable water level after tunnel construction, was delivered to the corresponding topsoil column. In each soil column, the topsoil model simulated unsaturated flow with a constant groundwater level. In transient cases, the groundwater model computed daily water level fluctuations during tunneling at each node and output the results of each node as a time

series. After resampling, the time series of daily average water levels for each block was delivered to the corresponding topsoil column. Subsequently, in each time step (i.e., one day) of topsoil simulations, one groundwater level was retrieved from the time series and imposed on the topsoil column as a fixed water head BC. The groundwater model considered the influences of water movements within the vadose zone on groundwater fluctuations using its built-in method, as shown in Eq. (6). Thus, the feedback (e.g., rainfall infiltration, soil evaporation, and root water uptake) from the topsoil to groundwater were neglected during the model coupling.

### 3.3. Regional vegetation vulnerability analysis

The regional vulnerability status of vegetation was assessed by applying vulnerability criteria (Section 2.3) to each block that depends on groundwater. If the groundwater level of a site is far below the plant rooting depth, vegetation in this zone can be inferred to be groundwater-independent (Eamus et al., 2006; 2016). In addition, plants can hardly extract sufficient moisture for ecological water demand when the groundwater table exceeds five meters (Ye et al., 2010; Chen et al., 2004; Hao et al., 2010; Rossatto et al., 2012). Thus, we assumed that the groundwater level threshold was ten times the plant rooting depth and no less than five meters. During the vulnerability analysis, blocks with initial groundwater levels lower than the threshold were excluded from the analyses.

#### 4. Case study and discussion

In this section, we apply the assessment framework to an actual tunnel project and evaluate the impact of its drainage on regional vegetation under different scenarios.

##### 4.1. Study site and model parameter values

The Mingtang Tunnel is a highway tunnel situated in Yuexi County, Anhui Province, mid-eastern China (Fig. 4(a)). This 7.548-km-long tunnel runs in an east-west direction ( $266^\circ$ – $272^\circ$ ) and is part of the Yue-wu highway that connects the cities of Wuhan and Shanghai. The tunnel was excavated using the drill-and-blast method. The burial depth of the tunnel varies from 322 m to 548 m, and the average depth is

**Table 1**  
Parameter values of the Mualem–van Genuchten soil water characteristic model.

| Soil type   | Depth (cm) | $\theta_s$ | $\theta_r$ | $\alpha$ | $n$  | $K_s$ (cm·d <sup>-1</sup> ) |
|-------------|------------|------------|------------|----------|------|-----------------------------|
| Clay loam*  | 0 ~ 50     | 0.41       | 0.095      | 0.019    | 1.31 | 6.24                        |
| Clay*       | 50 ~ 150   | 0.38       | 0.068      | 0.008    | 1.09 | 4.8                         |
|             | 350 ~ 5000 |            |            |          |      |                             |
| Silty clay* | 150 ~ 350  | 0.36       | 0.07       | 0.005    | 1.09 | 0.48                        |

\* Class average values for the Mualem–van Genuchten model from Carsel and Parrish (1988).

approximately 435 m. Fig. 4(b) illustrates the geological conditions along the tunnel axis. One watershed that encompasses part of a nature reserve was selected as the study site (Fig. 4(a)). A landcover map of the research area (Fig. 4(c)) with a spatial resolution of 30 m was obtained from the GlobeLand30 database (Chen et al., 2014; 2017). The field surveys for the study site indicated that the dominant forests are Chinese fir (*Cunninghamia lanceolata*) along with bamboo (*Phyllostachys pubescens*), and the main crops include rice, maize, and tea (Fig. 4(d)). Precipitation during spring and summer constitutes more than 70% of the annual precipitation, and the average annual precipitation is 1452.2 mm. The temperature in the Mingtang area varies from  $-15.2^\circ\text{C}$  to  $39.4^\circ\text{C}$ , with an average annual value of  $14.5^\circ\text{C}$ .

Table 1 summarizes the soil parameter values used in the topsoil model. A landcover map with a spatial resolution of 100 m (Fig. 3) was obtained by interpolation of the original map shown in Fig. 4(c). The new landcover map was used to resample the groundwater levels. Plant species in the research area were simplified into two dominant species: Chinese fir and rice. We assumed that the rooting depth,  $D_r$ , was 1.5 m for Chinese fir (Chen et al., 2013; Yu, 1997) and 0.3 m for rice (Li et al., 2017; Allen et al., 1998). In addition, both plants were assumed to have medium root density ( $R_{avg} = 0.1 \text{ cm}^{-3}$ ) with a shape-factor,  $b$ , equal to 2. According to data collected from the literature (Vogel et al., 2013; Li et al., 2014), the parameter values of the water stress response function,  $\delta(h)$ , for Chinese fir/rice were set as  $h_1 = 0/100 \text{ cm}$ ,  $h_2 = 0/55 \text{ cm}$ ,  $h_3(\text{high}) = -60/-160 \text{ cm}$ ,  $h_3(\text{low}) = -1200/-250 \text{ cm}$ , and

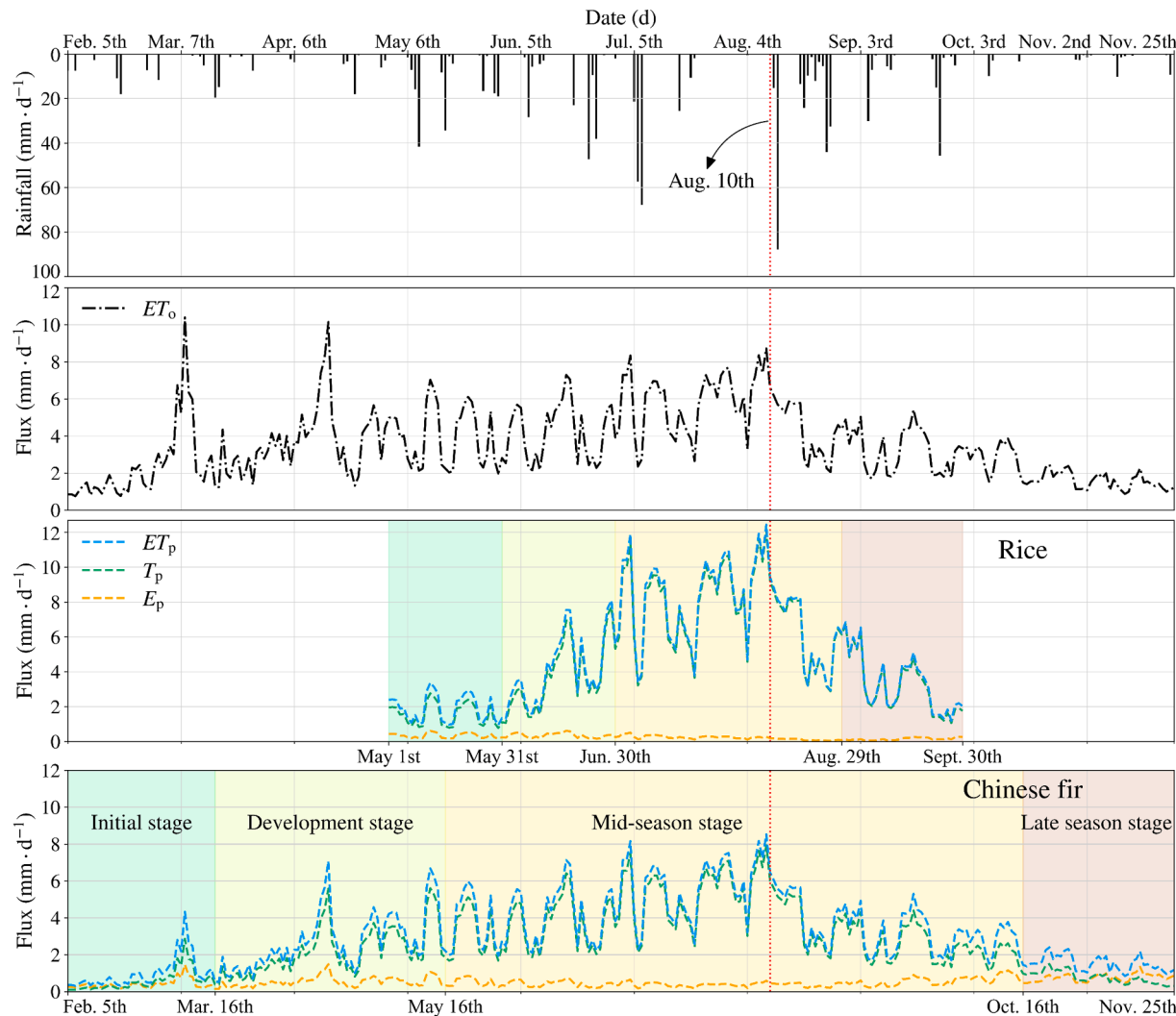


**Fig. 5.** Atmospheric forcing during growth stages of Chinese fir and rice in 2013–2014.

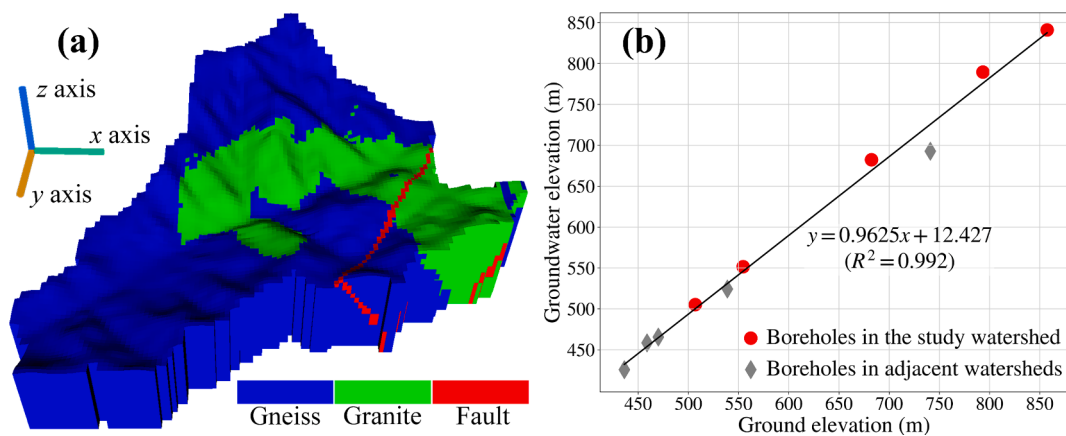


**Fig. 6.** (a) Lithological distribution used in the groundwater numerical simulations, (b) regression relationship between the ground surface elevation and groundwater elevation.

**Table 2**

Parameter values of the groundwater model.

| Based on in-situ and ex-situ data |  | Based on model calibration |  |
|-----------------------------------|--|----------------------------|--|
| Parameter                         | Value  | Parameter                  | Value  |
| Annual rainfall                   | 1452.2 mm  | $\lambda$                  | 2.8E-1   |
| Annual ET                         | 1418.3 mm  | $\xi$                      | 4.0E-1   |
| ET extinction depth               | 5.0 m below ground surface   | $\beta$                    | 4.5E-3 (steady-state)<br>2.5E-4 (steady-state, fault zone) |
| $\epsilon^*$                      | 16.2 <sup>i</sup>  |                            | 4.3E-2 (transient)   |
| $K_s^*$                           | 3.6E-2 <sup>i</sup>  |                            | 2.4E-3 (transient, fault zone)                             |
| $\theta_s^*$                      | 4.0E-2 <sup>i</sup>  |                            |  |
| $\theta_r^*$                      | 4.7E-1 <sup>i</sup>  |                            |  |
| B                                 | 6.3 <sup>ii</sup> (granite)<br>7.2 <sup>ii</sup> (gneiss)                  | A                          | -13.7 (granite)<br>-14.3 (gneiss)                          |
| C                                 | 595.6 <sup>ii</sup> (granite)<br>962.2 <sup>ii</sup> (gneiss)              |                            |  |
| $\mu_s$ (specific storage/yield)  | 6.9E-5/1.0E-2 <sup>ii</sup><br>6.9E-4/1.0E-1 <sup>ii</sup><br>(fault zone) | $\gamma$                   | 1.2E2  |

\* These are parameters of Brooks and Corey's model (1964), where  $\epsilon$  denotes the Brooks-Corey exponent, and the remaining parameters have the same meanings as those in the Mualem-van Genuchten model.

<sup>i</sup> Average values of silty clay loam (Brooks-Corey model) from Rawls et al. (1982).

<sup>ii</sup> Values from Li et al. (2018).

$h_w = -15,000$  cm. More information regarding the parameter values used in the topsoil model is provided by Li et al. (2020) and Gokdemir et al. (2019).

Meteorological data for the tunnel construction period (2013–2014) were collected from the Huoshan weather station (No. 58314). The atmospheric conditions during the tunnel operation stage were assumed to be the same as those during the construction stage. The atmospheric forcing throughout the vegetation growth stages is shown in Fig. 5. Precipitation ( $P$ ), potential evaporation ( $E_p$ ), and potential transpiration ( $T_p$ ) were imposed on the topsoil model as top BCs. We assumed that local farmers planted rice around May 1st and finished harvesting on Sept. 30th (Allen et al., 1998; Li et al., 2014). Chinese fir was assumed to grow from February to November and lie dormant in December and January (Yu, 1997). Vegetation growth was divided into four phases: initial, development, mid-season, and late-season stages (Allen et al., 1998).

Fig. 6(a) shows the lithological distribution of the groundwater model, which was simplified from the field measurements shown in Fig. 4(b). One regression equation with empirical coefficients  $A$ ,  $B$ , and  $C$ , i.e.,  $\log(K_{rock}) = A + B \cdot \exp(-x/C)$ , was used to calculate the rock hydraulic conductivity,  $K_{rock}$  ( $\text{m d}^{-1}$ ), based on the buried depth,  $x$  (m)

(Li et al., 2018).  $K_{rock}$  in the fault zone was assumed to be  $\gamma$  times that in the normal area (Yang et al., 2009). The initial groundwater elevations in the Mingtang area were strongly correlated to ground elevations (Fig. 6(b)). The groundwater model adopted annual  $P$  and  $ET$  as atmospheric forcing in the steady-state analyses, whereas  $P$  and  $ET_o$  that varied with time (shown in Fig. 5) were used for the transient simulations. In addition, to consider the effect of the unsaturated zone in transient cases, the top layer of the model was set as a homogenous soil layer with the texture of silty clay loam based on our previous studies (Li et al., 2020; Gokdemir et al., 2019). The distribution of rivers and streams was determined according to digital elevation model (DEM) data and field survey results. The parameter values for the groundwater model were determined based on field tests, ex-situ data, and model calibrations (Li et al., 2018), as listed in Table 2.

#### 4.2. Results and discussion

Several scenarios were designed to validate the applicability of the assessment framework. The simulated scenarios consisted of: (1) cases with different drainage rates or excavation speeds to compare the ecological influences of different design/construction parameters; (2) cases with varying aridity to validate whether the drainage of the Mingtang Tunnel would jeopardize vegetation during extreme situations (drought disasters); and (3) steady-state/transient cases to evaluate impacts during the operation/excitation phases.

##### 4.2.1. Comparison and optimization of tunnel parameters

In this section, using the discharge rate and excavation speed as examples, we demonstrate utilization of the regional assessment framework to compare and optimize tunnel design/construction parameters to minimize their impacts on vegetation. Along with the development of environmental philosophy, three typical design concepts for the waterproofing and drainage system (WDS) of mountain tunnels have emerged sequentially. These are the design concept without drainage limits, which emerged in the early stages (Li et al., 2016), the limited discharge design concept (Cheng et al., 2019; Gomes, 2005), and the design concept applicable for watertight tunnels constructed in regions with low groundwater levels (Gomes, 2005; Yuan et al., 2000). We used three steady-state drainage rates of 2585.45  $\text{m}^3/\text{d}$ , 950  $\text{m}^3/\text{d}$  (drainage rate of the Mingtang Tunnel), and 555.12  $\text{m}^3/\text{d}$  to compare the eco-environmental effects of different drainage schemes. Fig. 7 shows the most vulnerable results of the steady-state cases with different drainage design criteria. We defined vegetation within the watershed as the most vulnerable when the sum of the root wilting length in the whole basin reached the maximum value. Fig. 8(a) illustrates the variations in the area occupied by vulnerable plants

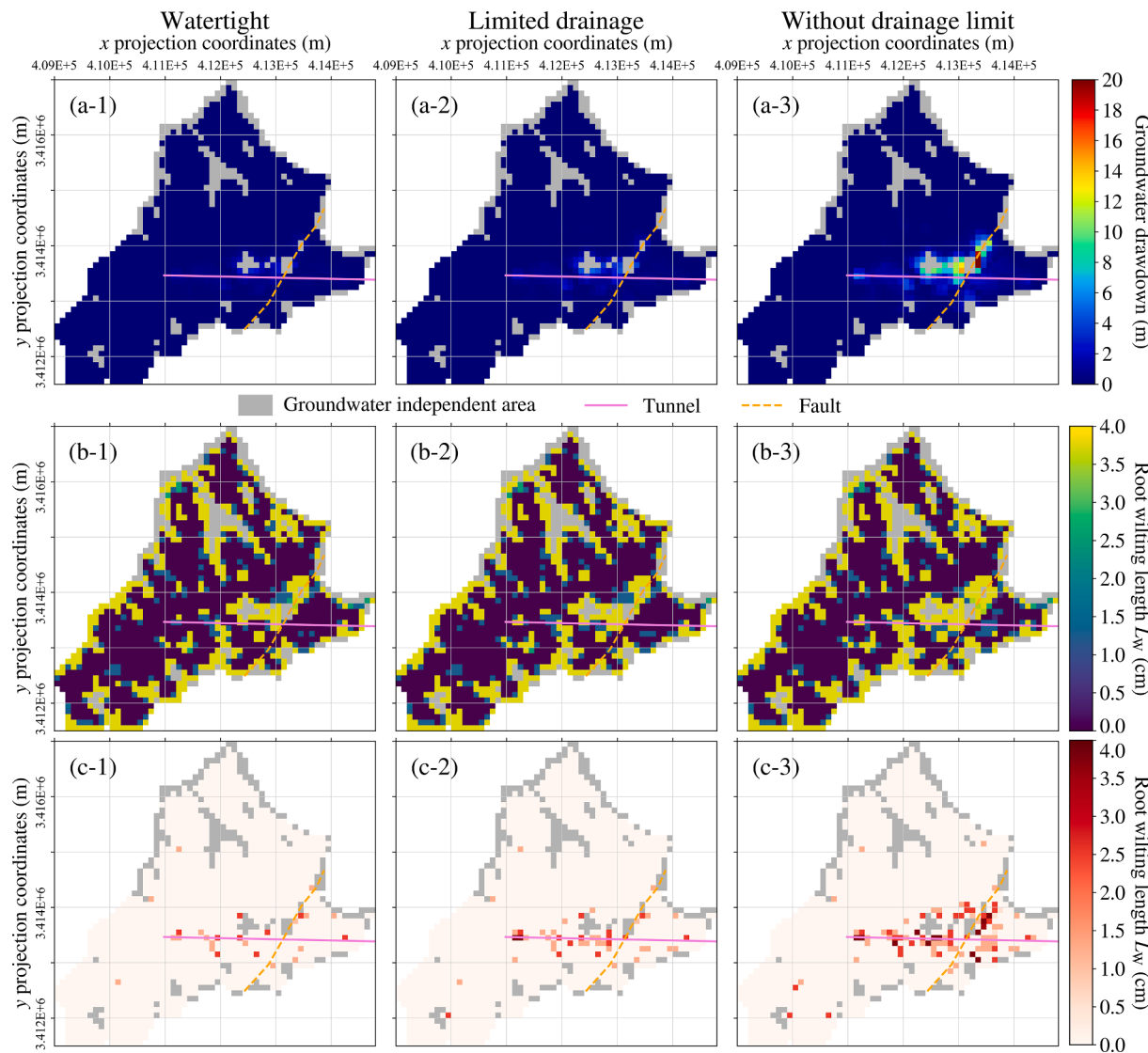


**Fig. 7.** Impacts of different steady-state tunnel drainage rates on plants (most vulnerable situations): (a) groundwater level drawdown after tunnel construction, (b) regional distributions of plant  $L_w$  after tunnel construction, and (c) root wilting caused by tunnel drainage.

throughout the vegetation growth stages when different drainage design criteria were adopted.

The results in Fig. 7 suggest that the drainage criteria in different design concepts affected the distribution of vulnerable plants. In cases with different drainage criteria, the area of vulnerable vegetation varied in a similar pattern (Fig. 8(a)). However, the vegetation distributing along the tunnel axis was more significantly threatened by tunnel drainage (Fig. 7(c)) because of severe groundwater drawdown in these zones (Fig. 7(a)). The area of vulnerable vegetation along the fault increased markedly (Fig. 7(c-3)) when the design concept without drainage limits was adopted. Designed according to the typical limited drainage design concept, the Mingtang Tunnel adopted shotcrete and grouting techniques to reinforce weak sections and used drainage pipes to discharge excessive groundwater. As a result, the groundwater inflow rate within the fault zone dropped from  $1269.2 \text{ m}^3/\text{d}$  to  $142.4 \text{ m}^3/\text{d}$ , and the vulnerable area in the research region decreased from 92 ha to 46 ha (Fig. 7(c-2)). With stricter waterproof solutions, the impact of tunnel drainage on vegetation can be further reduced, as shown in Fig. 7(c-1). However, the application of advanced waterproofing techniques can significantly increase the project budget. Moreover, a completely waterproof design may not be feasible in regions with high groundwater levels because of excessive pore water pressure (Wang et al., 2008).

Hence, designing WDS and optimizing drainage design criteria also involve cost-benefit analyses.

In the transient analyses, we performed numerical experiments at three different excavation speeds: 1 m/d, 5 m/d, and 10 m/d. These three assumed excavation speeds can represent tunnels constructed in extremely weak rock, fair rock, and extremely good rock, respectively. The excavation direction of the Mingtang Tunnel within the research area was from west to east. We assumed that the starting date of excavation was Feb. 5th, the same day as the Chinese fir starts to grow, and the starting point was at the west end of the tunnel. Fig. 9 presents the most vulnerable results for the case with an excavation speed of 5 m/d. Fig. 9(c) illustrates that the transient impact of tunnel drainage had little effect on the plants. In addition, as shown in Fig. 8(b), different excavation speeds had almost the same influence on the regional vulnerability status of the vegetation. Therefore, it may not be necessary to adjust the excavation speed of the Mingtang Tunnel solely for ecological reasons.

#### 4.2.2. Validation of drainage design criteria during drought disasters

In this section, we simulate cases with artificially reduced precipitation to validate whether the drainage criterion of the Mingtang Tunnel would wither vegetation in the case of drought disasters during the

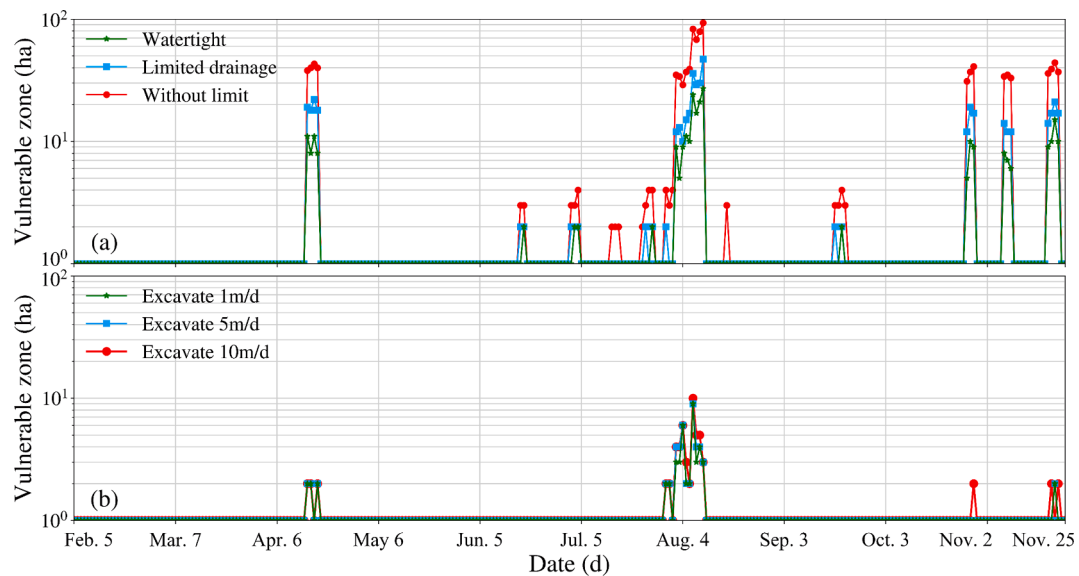


**Fig. 8.** Variations in the area of vulnerable vegetation caused or aggravated by tunnel drainage throughout the plant growth stages (all of the curves in this figure are artificially increased by one to adjust to the semi-logarithmic coordinate): (a) steady-state cases with different tunnel drainage criteria (the maximum value occurs on Aug. 10th), (b) transient cases with various tunnel excavation speeds (the maximum value occurs on Aug. 7th).

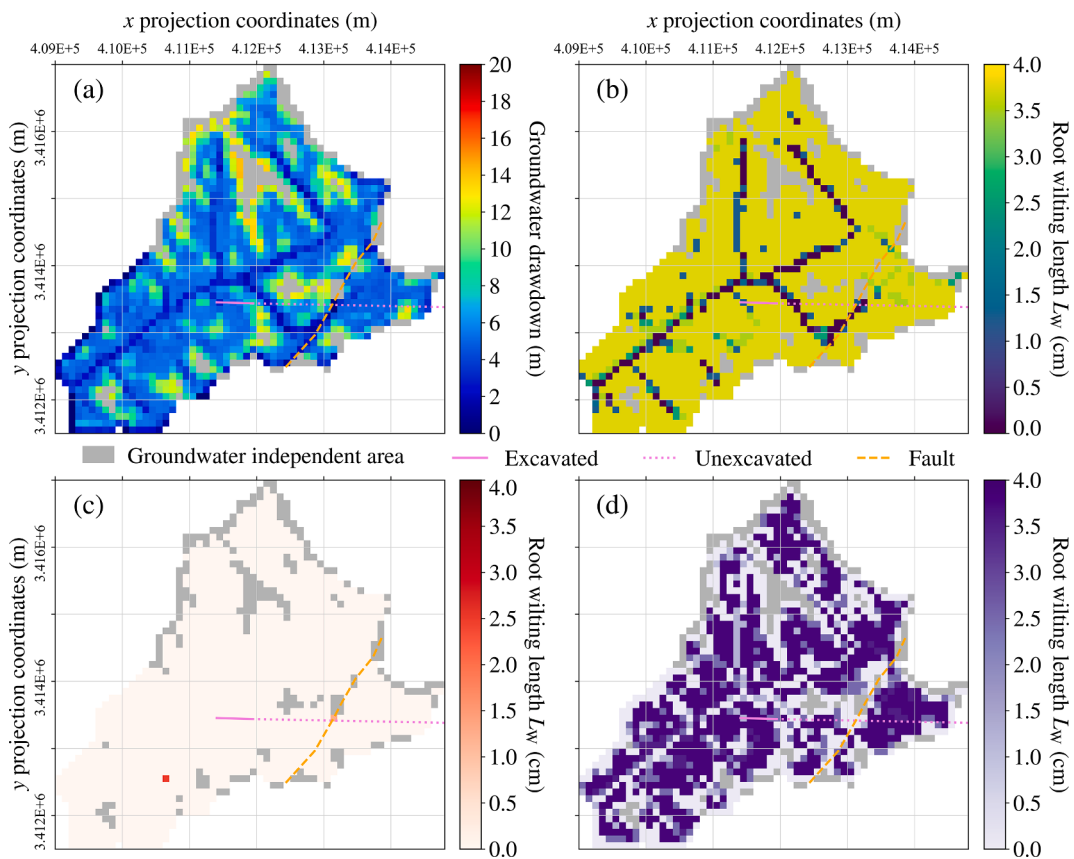


**Fig. 9.** Impact of transient tunnel drainage on vegetation when the excavation speed is 5 m/d (most vulnerable situation): (a) transient groundwater level drawdown, (b) regional distribution of plant  $L_w$  during construction, (c) plant root wilting caused by transient tunnel drainage, (d) plant root wilting caused by transient atmospheric conditions.

operation period. Here, we introduced the aridity index,  $AI (=P/ET_p)$ , to represent the degree of climate dryness at a given location (FAO, 1993; UNEP and Thomas, 1992). We simulated three scenarios with the reductions in rainfall of 10% ( $AI = 0.92$ , humid), 25% ( $AI = 0.77$ , sub-humid), and 50% ( $AI = 0.51$ , dry sub-humid/semi-arid). All three

simulations adopted the same limited drainage design ( $=950 \text{ m}^3/\text{d}$ ) as the Mingtang Tunnel. Fig. 10 shows the most vulnerable results for cases in which the rainfall was reduced to different degrees during the tunnel operation period. Even in severe drought disasters where the rainfall was reduced by 50% (Fig. 10(b-3)), the maximum  $L_w$  (11.25 cm) was

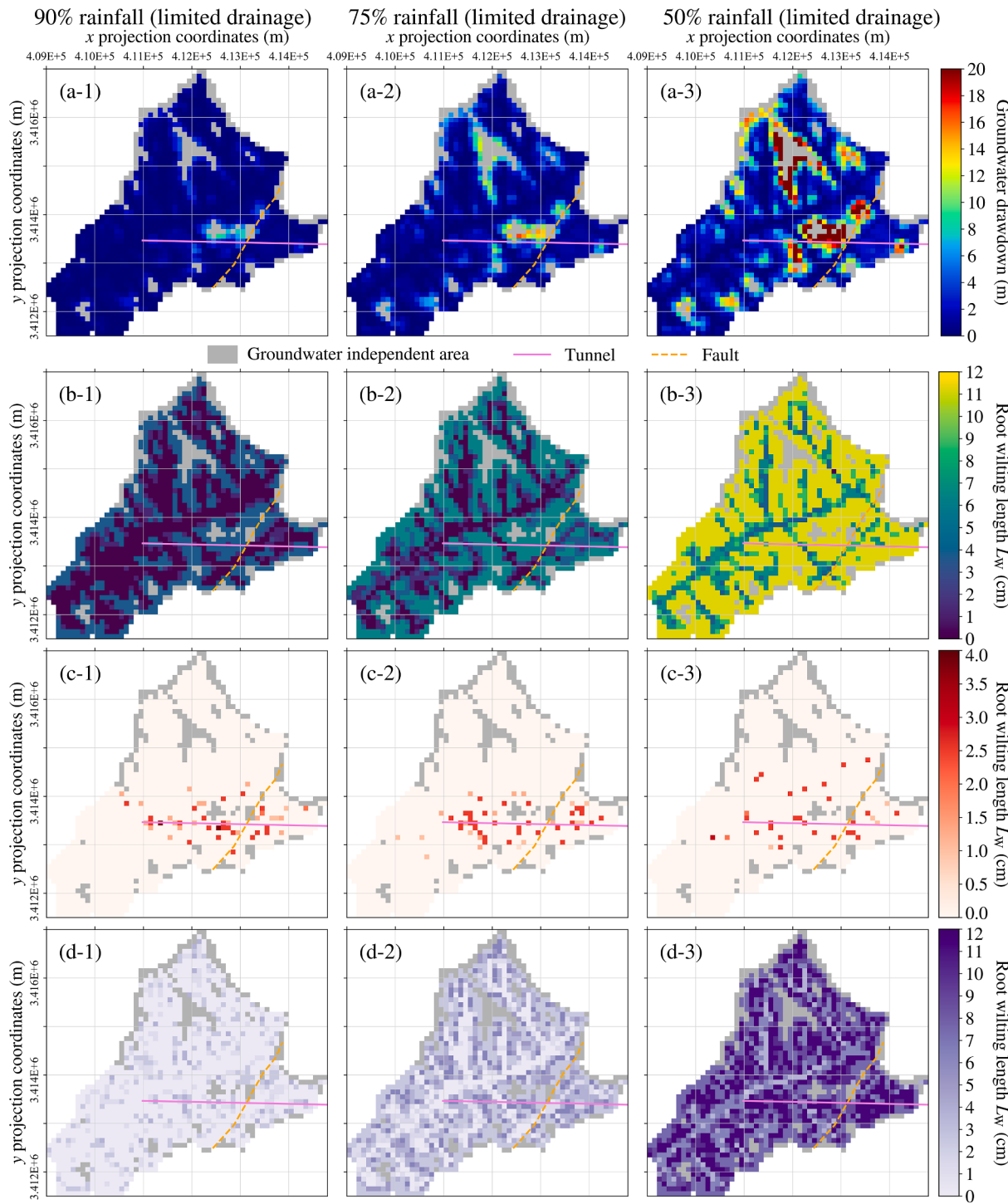


**Fig. 10.** Impacts of possible drought disasters on vegetation during the operation period (most vulnerable situation): (a) steady-state groundwater level drawdown, (b) regional distributions of plant  $L_w$ , (c) plant root wilting caused by tunnel drainage alone, (d) plant root wilting caused only by variations in atmospheric conditions.

less than half the rooting depth of Chinese fir or rice. Thus, we can speculate that the limited drainage criterion adopted by the Mingtang Tunnel would not wither vegetation during drought disasters.

#### 4.2.3. Dominant ecological factor: Tunnel drainage vs. Atmospheric conditions

In this section, we compare the regional impacts of tunnel drainage and atmospheric conditions on vegetation to determine which factor dominates vegetation vulnerability at the study site. As shown in Figs. 9

and 10, the area of vulnerable vegetation affected by atmospheric variations was much greater than that influenced by tunnel drainage. In addition, atmospheric conditions are highly correlated with the maximum  $L_w$  and the occurrence of the most vulnerable situation. The maximum  $L_w$  remained at 3.75 cm under the same normal atmospheric conditions (Fig. 7(b)), but increased along with the reduction in rainfall (5.5 cm, 6.25 cm, 11.25 cm for three cases in Fig. 10, respectively). According to the atmospheric BCs (Fig. 5), there was a three-week drought period before Aug. 10th, but both rice and Chinese fir thrived

during this period. The contradiction between the water supply (rainfall) and water consumption (evapotranspiration) during this phase led to the most vulnerable situation occurring on Aug. 10th for all evaluated cases. Hence, we conclude that both tunnel drainage and varying atmospheric conditions can make vegetation vulnerable, but atmospheric conditions have a more significant impact on the vegetation vulnerability status. This is also in agreement with the finding reported by Gokdemir et al. (2019) that root wilting is more dependent on infiltration.

#### 4.2.4. Regional impact of the Mingtang tunnel on vegetation

The analysis results suggest that plants did not wither during or after the construction of the Mingtang Tunnel. During normal atmospheric conditions, the maximum  $L_w$  was 3.75 cm (Fig. 7(b-2)), which is much less than the total rooting depth of Chinese fir (150 cm) and rice (30 cm). Even when severe drought disasters (rainfall reduced by 50%) occurred, the maximum  $L_w$  (11.75 cm) did not exceed the half-length of the total root (Fig. 10(b-3)). Moreover, the maximum  $L_w$  (3.75 cm) during tunnel construction (Fig. 9(b)) did not satisfy the second vulnerability criterion.

Tunnel drainage during the operation phase, however, did expand the area of vulnerable vegetation and exacerbated plant root wilting. As shown in Fig. 7(c-2), groundwater discharge from the Mingtang Tunnel during the operation period caused 27 ha of vegetation to become vulnerable and aggravated the vulnerability of 19 ha of plants. After the wilting point is met, vegetation growth may be stunted (Kirkham, 2014), and crop yields may be reduced (Fischer & Hagan, 1965; Stewart et al., 1977). Thus, groundwater discharge from the Mingtang Tunnel may have a detrimental effect on the growth and yield of 46 ha of plants during the operation period.

In contrast, groundwater inflow into the Mingtang Tunnel during the excavation process had a smaller effect on the vulnerability status of the vegetation. Tunnel drainage caused vegetation to be vulnerable for only 15 days of the entire growth stages of 294 days (Fig. 8(c)). In the most vulnerable situation, transient drainage led to only 2 ha of plants becoming (more) vulnerable (Fig. 9(c)).

## 5. Summary and conclusion

This study proposed an assessment framework to evaluate the regional impacts of tunnel drainage on vegetation. The framework evaluated the vulnerability status of vegetation by comparing the soil matric potential to the wilting point of plants. A quasi-3D numerical model, which connected the 3D groundwater levels with the 1D unsaturated flow through a one-way coupling method, was established to capture the regional distribution of the soil matric potential. By integrating the tunnel factor with SPAC, the framework could physically delineate water movements and ecological connections among the tunnel, groundwater, soil, plants, and atmosphere.

We applied the assessment framework to the Mingtang Tunnel and investigated the regional impact of its drainage on the surrounding vegetation. The results showed that the framework could compare and optimize tunnel design/construction parameters such as drainage design criteria and excavation speeds to minimize their ecological influences. For a specific tunnel, the framework can evaluate the regional impacts arising from its drainage during or after construction on the surrounding vegetation under normal or extreme atmospheric conditions. In addition, the framework can elucidate the relationships between environmental factors and identify the factors that control vegetation survival.

For the Mingtang Tunnel, we found that the area of vulnerable vegetation affected by tunnel drainage would diminish notably when the limited discharge solution of three typical drainage schemes was adopted. The Mingtang Tunnel with the controlled drainage scheme may decrease vegetation growth and yield in some zones, but it is unlikely to lead to wilting, even during drought disasters. Moreover, we revalidated that the vulnerability status of vegetation at the study site depends more on atmospheric conditions than tunnel drainage.

This paper presents a novel insight into the eco-environmental influences of tunnel engineering and a practical tool for their quantitative evaluation. In future work, we will focus on including the uncertainty of soil parameters in the current framework and obtaining a regional risk map of vegetation affected by tunnel drainage.

## CRediT authorship contribution statement

**Hao Xu:** Conceptualization, Methodology, Software, Formal analysis, Investigation, Data curation, Visualization, Writing - original draft.  
**Xiaojun Li:** Supervision, Resources, Writing - review & editing.  
**Cagri Gokdemir:** Investigation.

## Declaration of Competing Interest

The authors declare that they have no known competing financial interests or personal relationships that could have appeared to influence the work reported in this paper.

## Acknowledgments

This research was conducted with support from the Natural Science Foundation of China (Grant No. 41877246), the Science and Technology Plan Project of the Ministry of Transport of China (2013318J02120), the Tongji Civil Engineering Peak Discipline Plan, and the Fundamental Research Funds for Central Universities.

## References

- Abbott, M.B., Bathurst, J.C., Cunge, J.A., O'connell, P.E., Rasmussen, J., 1986. An introduction to the European Hydrological System-Système Hydrologique Européen, "SHE", 2: Structure of a physically-based, distributed modelling system. *J. Hydrol.* 87 (1–2), 61–77. [https://doi.org/10.1016/0022-1694\(86\)90115-0](https://doi.org/10.1016/0022-1694(86)90115-0).
- Adams, R., Younger, P.L., 2001. A strategy for modeling ground water rebound in abandoned deep mine systems. *Groundwater* 39 (2), 249–261. <https://doi.org/10.1111/j.1745-6584.2001.tb02306.x>.
- Allen, R.G., Pereira, L.S., Raes, D., Smith, M., 1998. Crop evapotranspiration-Guidelines for computing crop water requirements-FAO Irrigation and drainage paper 56. Food and Agriculture Organization of the United Nations, Rome. <http://www.fao.org/3/x0490e/x0490e00.htm>.
- Arnold, J.G., Srinivasan, R., Mutiah, R.S., Williams, J.R., 1998. Large area hydrologic modeling and assessment part I: model development 1. *J. Am. Water Resour. Assoc.* 34 (1), 73–89. <https://doi.org/10.1111/j.1752-1688.1998.tb05961.x>.
- Assi, A.T., Blake, J., Mohtar, R.H., Braudeau, E., 2019. Soil aggregates structure-based approach for quantifying the field capacity, permanent wilting point and available water capacity. *Irrig. Sci.* 37 (4), 511–522. <https://doi.org/10.1007/s00271-019-00630-w>.
- Audi, Y., Jullien, A., Dauvergne, M., Feraille, A., Schwartzenbauer, L.D.A., 2020. Methodology and application for the environmental assessment of underground multimodal tunnels. *Transp. Geotech.* 24, 100389 <https://doi.org/10.1016/j.trgeo.2020.100389>.
- Belmans, C., Wesseling, J.G., Feddes, R.A., 1983. Simulation model of the water balance of a cropped soil: SWATRE. *J. Hydrol.* 63 (3–4), 271–286. [https://doi.org/10.1016/0022-1694\(83\)90045-8](https://doi.org/10.1016/0022-1694(83)90045-8).
- Bobylev, N., 2006. Strategic environmental assessment of urban underground infrastructure development policies. *Tunn. Undergr. Space Technol.* 21 (3–4) <https://doi.org/10.1016/j.tust.2005.12.106>.
- Bobylev, N., 2018. Geosystem and ecosystem services – Exploring opportunities for inclusion in urban underground space planning. *ACUUS 2018 - 16th World Conference of the Associated Research Centers for the Urban Underground Space: Integrated Underground Solutions for Compact Metropolitan Cities* 238–248. [http://refhub.elsevier.com/S0264-8377\(19\)31316-X/sref0105](http://refhub.elsevier.com/S0264-8377(19)31316-X/sref0105).
- Brooks, R.H., Corey, A.T., 1964. Hydraulic properties of porous media and their relation to drainage design. *Transactions of the ASAE* 7 (1), 26–0028. <https://doi.org/10.13031/2013.40684>.
- Butscher, C., 2012. Steady-state groundwater inflow into a circular tunnel. *Tunnelling and Underground Space Technology* 32, 158–167. <https://doi.org/10.1016/j.tust.2012.06.007>.
- Carsel, R.F., Parrish, R.S., 1988. Developing joint probability distributions of soil water retention characteristics. *Water Resour. Res.* 24 (5), 755–769. <https://doi.org/10.1029/WR024i005p00755>.
- Chen, G.S., Yang, Z.J., Gao, R., Xie, J.S., Guo, J.F., Huang, Z.Q., Yang, Y.S., 2013. Carbon storage in a chronosequence of Cunninghamia lanceolata plantations in southern China. *Forest Ecol. Manag.* 300, 68–76. <https://doi.org/10.1016/j.foreco.2012.07.046>.
- Chen, J., Ban, Y., Li, S., 2014. Open access to Earth land-cover map. *Nature* 514 (7523), 434–434. <https://doi.org/10.1038/514434c>.

- Chen, J., Cao, X., Peng, S., Ren, H., 2017. Analysis and applications of GlobeLand30: a review. *ISPRS Int. J. Geo-Inf.* 6 (8), 230. <https://doi.org/10.3390/ijgi6080230>.
- Chen, Y., Li, W., Chen, Y., Zhang, H., Zhuang, L., 2004. Physiological response of natural plants to the change of groundwater level in the lower reaches of Tarim River. Xinjiang. *Progress in Natural Science* 14 (11), 975–983. <https://doi.org/10.1080/10020070412331344661>.
- Cheng, P., Zhao, L., Luo, Z., Li, L., Li, Q., Deng, X., Peng, W., 2019. Analytical solution for the limiting drainage of a mountain tunnel based on area-well theory. *Tunn. Undergr. Space Technol.* 84, 22–30. <https://doi.org/10.1016/j.tust.2018.10.014>.
- Consoli, S., Stagno, F., Vanella, D., Boaga, J., Cassiani, G., Roccuzzo, G., 2017. Partial root-zone drying irrigation in orange orchards: Effects on water use and crop production characteristics. *Eur. J. Agron.* 82, 190–202. <https://doi.org/10.1016/j.eja.2016.11.001>.
- Daily, G.C., 1997. *Nature's services: Societal dependence on natural ecosystems*. Island Press, Washington, DC.
- Emam, D., Froend, R., Loomes, R., Hose, G., Murray, B., 2006. A functional methodology for determining the groundwater regime needed to maintain the health of groundwater-dependent vegetation. *Aust. J. Bot.* 54 (2), 97–114. <https://doi.org/10.1071/BT05031>.
- Emam, D., Fu, B., Springer, A.E., Stevens, L.E., 2016. Groundwater dependent ecosystems: classification, identification techniques and threats. *Integrated Groundwater Management*. Springer, pp. 313–346. [https://doi.org/10.1007/978-3-319-23576-9\\_13](https://doi.org/10.1007/978-3-319-23576-9_13).
- Fais, A.A., Nino, P.P., 2004. Diachronic land-use analysis for the evaluation of the impact on agriculture and natural vegetation of the high-speed railway tunnel in central Italy. *International Society for Optics and Photonics* 5544, 286–294. <https://doi.org/10.1117/12.557625>.
- FAO, 1993. *Forest Resources Assessment 1990. Tropical Countries. Forestry Paper 112. Food and Agriculture Organization of the United Nations (FAO)*, Rome.
- Feddes, R., Kowalik, P., & Zaradny, H. (1978). Simulation of field water use and crop yield. *Simulation Monograph Series*, Pudoc, Wageningen, the Netherlands.
- Fischer, R.A., Hagan, R.M., 1965. Plant water relations, irrigation management and crop yield. *Exp. Agric.* 1 (3), 161–177. <https://doi.org/10.1017/S0014479700021402>.
- UNEP, N.M., Thomas, D., 1992. *World atlas of desertification*. Edward Arnold, London, pp. 15–45.
- van Genuchten, M.T., 1980. A closed-form equation for predicting the hydraulic conductivity of unsaturated soils. *Soil Sci. Soc. Am. J.* 44 (5), 892. <https://doi.org/10.2136/sssaj1980.03615995004400050002x>.
- van Geldermalsen, L.A., 2004. Environmental aspects in tunnel design. *1st International Symposium, Prague 199–210*.
- García-Nieto, A.P., García-Llorente, M., Iniesta-Arandia, I., Martín-López, B., 2013. Mapping forest ecosystem services: from providing units to beneficiaries. *Ecosyst. Serv.* 4, 126–138. <https://doi.org/10.1016/j.ecoser.2013.03.003>.
- Gargini, A., Vincenzi, V., Piccinini, L., Zuppi, G.M., Canuti, P., 2008. Groundwater flow systems in turbidites of the Northern Apennines (Italy): natural discharge and high speed railway tunnel drainage. *Hydrogeol. J.* 16 (8), 1577–1599. <https://doi.org/10.1007/s10040-008-0352-8>.
- Gokdemir, C., Rubin, Y., Li, X., Li, Y., Xu, H., 2019. Vulnerability analysis method of vegetation due to groundwater table drawdown induced by tunnel drainage. *Adv. Water Resour.* 133, 103406. <https://doi.org/10.1016/j.advwatres.2019.103406>.
- Gomes, A.R., 2005. *Waterproofing and Drainage Systems for Transport Tunnels—A Review of Current Practices*. Felsbau 23 (3), 46–49.
- Hanks, R.J., 1992. *Applied soil physics: soil water and temperature applications (Second Edition)*. Springer.
- Hanson, R.T., Boyce, S.E., Schmid, W., Hughes, J.D., Mehl, S.W., Leake, S.A., Niswonger, R.G., 2014. One-water hydrologic flow model (MODFLOW-OWHM) (No. 6-A51). United States Geological Survey. <https://doi.org/10.3133/tm6A51>.
- Hao, X., Li, W., Huang, X., Zhu, C., Ma, J., 2010. Assessment of the groundwater threshold of desert riparian forest vegetation along the middle and lower reaches of the Tarim River. *China. Hydrological Processes: An International Journal* 24 (2), 178–186. <https://doi.org/10.1002/hyp.7432>.
- Harbaugh, A.W., 2005. MODFLOW-2005, the US Geological Survey modular groundwater model: the groundwater flow process (6-A16). United States Geological Survey. <https://doi.org/10.3133/tm6A16>.
- Hsiao, T.C., 1973. Plant responses to water stress. *Annu. Rev. Plant Physiol.* 24 (1), 519–570. <https://doi.org/10.1146/annurev.pp.24.060173.002511>.
- Huang, L., Bohne, R.A., Bruland, A., Jakobsen, P.D., Lohne, J., 2015. Life cycle assessment of Norwegian road tunnel. *The International Journal of Life Cycle Assessment* 20 (2), 174–184. <https://doi.org/10.1007/s11367-014-0823-1>.
- Jansson, P.E., 2012. CoupModel: model use, calibration, and validation. *Trans. ASABE* 55 (4), 1337–1344. <https://doi.org/10.13031/2013.42245>.
- Jensen, M.E., Allen, R.G., 2016. Evaporation, evapotranspiration, and irrigation water requirements. American Society of Civil Engineers. <https://doi.org/10.1061/9780784414057>.
- Kirkham, M.B., 2014. *Principles of soil and plant water relations*. Academic Press. <https://doi.org/10.1016/C2013-0-12871-1>.
- Krieger, D., 2001. *Economic value of forest ecosystem services: a review*. The Wilderness Society, Washington DC.
- Kroes, J.G., van Dam, Bartholomeus, R.P., Groenendijk, P., Heinen, M., Hendriks, R.F.A., et al., 2017. SWAP version 4: Theory description and user manual. Wageningen Environmental Research. <https://doi.org/10.18174/416321>.
- Kværner, J., Snilsberg, P., 2008. The Romeriksporlen railway tunnel—drainage effects on peatlands in the lake Northern Putjern area. *Eng. Geol.* 101 (3–4), 75–88. <https://doi.org/10.1016/j.enggeo.2008.04.002>.
- Kværner, J., Snilsberg, P., 2011. Groundwater hydrology of boreal peatlands above a bedrock tunnel—Drainage impacts and surface water groundwater interactions. *J. Hydrol.* 403 (3–4), 278–291. <https://doi.org/10.1016/j.jhydrol.2011.04.006>.
- Li, L., Tu, W., Shi, S., Chen, J., Zhang, Y., 2016. Mechanism of water inrush in tunnel construction in karst area. *Geomatics, Natural Hazards and Risk* 7 (sup1), 35–46. <https://doi.org/10.1080/19475705.2016.1181342>.
- Li, S., Zuo, Q., Wang, X., Ma, W., Jin, X., Shi, J., Ben-Gal, A., 2017. Characterizing roots and water uptake in a ground cover rice production system. *PLoS ONE* 12 (7). <https://doi.org/10.1371/journal.pone.0180713>.
- Li, X., Li, Y., Chang, C.F., Tan, B., Chen, Z., Sege, J., Wang, C., Rubin, Y., 2018. Stochastic, goal-oriented rapid impact modeling of uncertainty and environmental impacts in poorly-sampled sites using ex-situ priors. *Adv. Water Resour.* 111, 174–191. <https://doi.org/10.1016/j.advwatres.2017.11.008>.
- Li, X., Xu, H., Gokdemir, C., Wang, F., Huang, X., 2020. TSPAC analysis method for the impact of groundwater drawdown induced by tunnel drainage on terrestrial vegetation. *Tunnel. Construction* 40 (9), 1261–1271. <https://doi.org/10.3973/j.issn.2096-4498.2020.09.003> (in Chinese).
- Li, Y., Šimunek, J., Jing, L., Zhang, Z., Ni, L., 2014. Evaluation of water movement and water losses in a direct-seeded-rice field experiment using Hydrus-1D. *Agric. Water Manag.* 142, 38–46. <https://doi.org/10.1016/j.agwat.2014.04.021>.
- Liu, D., Yang, L., Yu, S., 2001. On ecological environment problems and effects caused by discharge from Huayingshan Tunnel. *Journal of Southwest Jiaotong University* 36 (3), 308–313. <https://doi.org/10.3969/j.issn.0258-2724.2001.03.021> (in Chinese).
- Liu, J., Liu, D., Song, K., 2015. Evaluation of the influence caused by tunnel construction on groundwater environment: A case study of Tongluoshan tunnel, China. *Adv. Mater. Sci. Eng.* 2015, 149265. <https://doi.org/10.1155/2015/149265>.
- Liu, J., Shen, L., Wang, Z., Duan, S., Wu, W., Peng, X., Wu, C., Jiang, Y., 2019. Response of plants water uptake patterns to tunnels excavation based on stable isotopes in a karst trough valley. *J. Hydrol.* 571, 485–493. <https://doi.org/10.1016/j.jhydrol.2019.01.073>.
- Lv, Y., Jiang, Y., Hu, W., Cao, M., Mao, Y., 2020. A review of the effects of tunnel excavation on the hydrology, ecology, and environment in karst areas: Current status, challenges, and perspectives. *J. Hydrol.* 124891. <https://doi.org/10.1016/j.jhydrol.2020.124891>.
- Mao, W., Zhu, Y., Dai, H., Ye, M., Yang, J., Wu, J., 2019. A comprehensive quasi-3-D model for regional-scale unsaturated-saturated water flow. *Hydrol. Earth Syst. Sci.* 23 (8), 3481–3502. <https://doi.org/10.5194/hess-23-3481-2019>.
- Markstrom, S.L., Niswonger, R.G., Regan, R.S., Prudic, D.E., Barlow, P.M., 2008. GSFLOW—coupled ground-water and surface-water flow model based on the integration of the precipitation-runoff modeling system (PRMS) and the modular ground-water flow model (MODFLOW-2005). United States Geological Survey.
- McElrone, A.J., Choat, B., Gambetta, G.A., Brodersen, C.R., 2013. Water uptake and transport in vascular plants. *Nature Education Knowledge* 4 (6).
- Millennium Ecosystem Assessment, 2005. *Ecosystems and human well-being*. World Resources Institute, Washington DC.
- Moon, J., Fernandez, G., 2010. Effect of excavation-induced groundwater level drawdown on tunnel inflow in a jointed rock mass. *Eng. Geol.* 110 (3–4), 33–42. <https://doi.org/10.1016/j.enggeo.2009.09.002>.
- Mualem, Y., 1976. A new model for predicting the hydraulic conductivity of unsaturated porous media. *Water Resour. Res.* 12 (3), 513–522. <https://doi.org/10.1029/WR012i003p00513>.
- Namin, F.S., Ghafari, H., Dianati, A., 2014. New model for environmental impact assessment of tunneling projects. *Journal of Environmental Protection* 5, 530–550. <https://doi.org/10.4236/jep.2014.50506>.
- Nemali, K., Stephens, M., 2014. Plant Abiotic Stress: Water. *Encyclopedia of Agriculture and Food Systems* 4, 335–342. <https://doi.org/10.1016/B978-0-444-52512-3.00170-4>.
- Neuman, S.P., Feddes, R.A., Bresler, E., 1975. Finite element analysis of two-dimensional flow in soils considering water uptake by roots: I. Theory. *Soil Sci. Soc. Am. J.* 39 (2), 224–230. <https://doi.org/10.2136/sssaj1975.03615995003900020007x>.
- Niswonger, R.G., Prudic, D.E., Regan, R.S., 2006. Documentation of the unsaturated-zone flow (UZF1) package for modeling unsaturated flow between the land surface and the water table with MODFLOW-2005 (No. 6-A19). United States Geological Survey. <https://doi.org/10.3133/tm6A19>.
- Niswonger, R.G., Panday, S., Ibaraki, M., 2011. MODFLOW-NWT, a Newton formulation for MODFLOW-2005 (No. 6-A37). United States Geological Survey. <https://doi.org/10.3133/tm6A37>.
- Pan, Y., Gong, H., Sun, Y., Wang, X., Ding, F., 2017. Distributed estimation and analysis of precipitation recharge coefficient in strongly-exploited Beijing plain area, China. *Chinese Geographical Science* 27 (1), 88–96. <https://doi.org/10.1007/s11769-016-0839-5>.
- Philip, J.R., 1966. Plant water relations: some physical aspects. *Annu. Rev. Plant Physiol.* 17 (1), 245–268. <https://doi.org/10.1146/annurev. pp. 17.060166.001333>.
- Phillips, J., 2016. A quantitative evaluation of the sustainability or unsustainability of three tunnelling projects. *Tunn. Undergr. Space Technol.* 51, 387–404. <https://doi.org/10.1016/j.tust.2015.09.009>.
- Porporato, A., Laio, F., Ridolfi, L., Rodriguez-Iturbe, I., 2001. Plants in water-controlled ecosystems: active role in hydrologic processes and response to water stress: III. Vegetation water stress. *Adv. Water Resour.* 24 (7), 725–744. [https://doi.org/10.1016/S0309-1708\(01\)00006-9](https://doi.org/10.1016/S0309-1708(01)00006-9).
- Qiu, W., Liu, Y., Lu, F., Huang, G., 2020. Establishing a sustainable evaluation indicator system for railway tunnel in China. *J. Cleaner Prod.* 268, 122150. <https://doi.org/10.1016/j.jclepro.2020.122150>.
- Raposo, J.R., Molinero, J., Dafonte, J., 2010. Quantitative evaluation of hydrogeological impact produced by tunnel construction using water balance models. *Eng. Geol.* 116 (3–4), 323–332. <https://doi.org/10.1016/j.enggeo.2010.09.014>.

- Rangarajan, R., Athavale, R.N., 2000. Annual replenishable ground water potential of India—an estimate based on injected tritium studies. *J. Hydrol.* 234 (1–2), 38–53. [https://doi.org/10.1016/S0022-1694\(00\)00239-0](https://doi.org/10.1016/S0022-1694(00)00239-0).
- Rawls, W.J., Brakensiek, D.L., Saxton, K.E., 1982. Estimation of soil water properties. *Transactions of the ASAE* 25 (5), 1316–1320. <https://doi.org/10.13031/2013.33720>.
- Ritchie, J.T., 1972. Model for predicting evaporation from a row crop with incomplete cover. *Water Resour. Res.* 8 (5), 1204–1213. <https://doi.org/10.1029/WR008i005p01204>.
- Robinson, M., Ward, R.C., 2017. Hydrology: principles and processes. Iwa Publishing. <https://doi.org/10.2166/9781780407296>.
- Rossatto, D.R., Silva, L.D.C.R., Villalobos-Vega, R., Sternberg, L.D.S.L., Franco, A.C., 2012. Depth of water uptake in woody plants relates to groundwater level and vegetation structure along a topographic gradient in a neotropical savanna. *Environ. Exp. Bot.* 77, 259–266. <https://doi.org/10.1016/j.enexpbot.2011.11.025>.
- Santos, M.A.D., van Lier, J., Dam, J.C.V., Freire Bezerra, A.H., 2017. Benchmarking test of empirical root water uptake models. *Hydrol. Earth Syst. Sci.* 21 (1), 473–493. <https://doi.org/10.5194/hess-21-473-2017>.
- Seo, H.S., Simunek, J., Poeter, E.P., 2007. Documentation of the hydrus package for modflow-2000, the US Geological Survey modular groundwater model. International Ground Water Modeling Center.
- Šimůnek, J., Šejna, M., Saito, M., Sakai, M., van Genuchten, M.T., 2009. The HYDRUS-1D software package for simulating the one-dimensional movement of water, heat, and multiple solutes in variably-saturated media (version 4.08). Department of Environmental Sciences University of California-Riverside.
- Stewart, J.I., Danielson, R.E., Hanks, R.J., Jackson, E.B., Hagan, R.M., Pruitt, W.O., Franklin, W.T., Riley, J.P., 1977. Optimizing crop production through control of water and salinity levels in the soil. Utah Water Research Laboratory, Utah State University.
- Sweetenham, M.G., Maxwell, R.M., Santi, P.M., 2017. Assessing the timing and magnitude of precipitation-induced seepage into tunnels bored through fractured rock. *Tunn. Undergr. Space Technol.* 65, 62–75. <https://doi.org/10.1016/j.tust.2017.02.003>.
- Toran, L., Bradbury, K.R., 1988. Groundwater flow model of drawdown and recovery near an underground mine. *Groundwater* 26 (6), 724–733. <https://doi.org/10.1111/j.1745-6584.1988.tb00423.x>.
- Vincenzi, V., Gargini, A., Goldscheider, N., 2009. Using tracer tests and hydrological observations to evaluate effects of tunnel drainage on groundwater and surface waters in the Northern Apennines (Italy). *Hydrogeol. J.* 17 (1), 135–150. <https://doi.org/10.1007/s10040-008-0371-5>.
- Vogel, T., Dohnal, M., Dusek, J., Votruba, J., Tesar, M., 2013. Macroscopic modeling of plant water uptake in a forest stand involving root-mediated soil water redistribution. *Vadose Zone J.* 12 (1) <https://doi.org/10.2136/vzj2012.0154>.
- Wang, X., Wang, M., Zhang, M., Ming, H., 2008. Theoretical and experimental study of external water pressure on tunnel lining in controlled drainage under high water level. *Tunn. Undergr. Space Technol.* 23 (5), 552–560. <https://doi.org/10.1016/j.tust.2007.10.004>.
- Ward, A.D., Trimble, S.W., 2003. *Environmental hydrology*. CRC Press.
- Wei, D., Pan, J., 2011. Dynamic Monitoring of the Ecoenvironment Influence of Tunnel Construction Based on Remote Sensing. *Geospatial. Information* 9 (1), 16–19. <https://doi.org/10.3969/j.issn.1672-4623.2011.01.006> (in Chinese).
- Xu, X., Huang, G., Zhan, H., Qu, Z., Huang, Q., 2012. Integration of SWAP and MODFLOW-2000 for modeling groundwater dynamics in shallow water table areas. *J. Hydrol.* 412, 170–181. <https://doi.org/10.1016/j.jhydrol.2011.07.002>.
- Xu, Y.S., Shen, S.L., Ren, D.J., Wu, H.N., 2016. Analysis of factors in land subsidence in Shanghai: a view based on a strategic environmental assessment. *Sustainability* 8 (6), 573. <https://doi.org/10.3390/su8060573>.
- Yadvinder-Singh, Kukal, S.S., Jat, M.L., Sidhu, H.S., 2014. Improving Water Productivity of Wheat-Based Cropping Systems in South Asia for Sustained Productivity. *Adv. Agron.* 127, 157–258. <https://doi.org/10.1016/B978-0-12-800131-8.00004-2>.
- Yang, F.R., Lee, C.H., Kung, W.J., Yeh, H.F., 2009. The impact of tunneling construction on the hydrogeological environment of “Tseng-Wen Reservoir Transbasin Diversion Project” in Taiwan. *Eng. Geol.* 103 (1–2), 39–58. <https://doi.org/10.1016/j.enggeo.2008.07.012>.
- Ye, Z., Chen, Y., Li, W., 2010. Ecological water demand of natural vegetation in the lower Tarim River. *J. Geog. Sci.* 20 (2), 261–272. <https://doi.org/10.1007/s11442-010-0261-3>.
- Yoo, C., 2005. Interaction between tunneling and groundwater—numerical investigation using three dimensional stress–pore pressure coupled analysis. *J. Geotech. Geoenviron. Eng.* 131 (2), 240–250. [https://doi.org/10.1061/\(ASCE\)1090-0241\(2005\)131:2\(240\)](https://doi.org/10.1061/(ASCE)1090-0241(2005)131:2(240)).
- Yu, X., 1997. *Cunninghamia lanceolata cultivation*. Fujian Science & Technology Publishing House. (in Chinese).
- Yuan, Y., Jiang, X., Lee, C.F., 2000. Tunnel waterproofing practices in China. *Tunn. Undergr. Space Technol.* 15 (2), 227–233. [https://doi.org/10.1016/S0886-7798\(00\)00048-1](https://doi.org/10.1016/S0886-7798(00)00048-1).
- Zaidel, J., Markham, B., Bleiker, D., 2010. Simulating seepage into mine shafts and tunnels with MODFLOW. *Groundwater* 48 (3), 390–400. <https://doi.org/10.1111/j.1745-6584.2009.00659.x>.
- Zargarian, R., Hunt, D.V., Braithwaite, P., Bobylev, N., Rogers, C.D., 2016. A new sustainability framework for urban underground space. *Proceedings of the Institution of Civil Engineers: Engineering Sustainability* 171 (5), 238–253. <https://doi.org/10.1680/jensu.15.00013>.
- Zeng, J., Yang, J., Zha, Y., Shi, L., 2019. Capturing soil–water and groundwater interactions with an iterative feedback coupling scheme: new HYDRUS package for MODFLOW. *Hydrol. Earth Syst. Sci.* 23 (2), 637–655. <https://doi.org/10.5194/hess-23-637-2019>.
- Zhang, G., Qian, W., Wu, F., 2012. Research on water ecology of tunnel engineering in arid and semi-arid regions. *Applied Mechanics and Materials* 212, 647–652. <https://www.scientific.net/AMM.212-213.647>.
- Zheng, W., Wang, X., Tang, Y., Liu, H., Wang, M., Zhang, L., 2017. Use of tree rings as indicator for groundwater level drawdown caused by tunnel excavation in Zhongliang Mountains, Chongqing, Southwest China. *Environmental Earth Sciences* 76 (15), 522. <https://doi.org/10.1007/s12665-017-6859-3>.
- Zotarelli, L., Dukes, M.D., Romero, C.C., Migliaccio, K.W., Morgan, K.T., 2010. Step by step calculation of the Penman-Monteith Evapotranspiration (FAO-56 Method). Institute of Food and Agricultural Sciences, University of Florida.